One-dimensional modeling of necking in rate-dependent materials

Basile Audoly [a,b,*], John W. Hutchinson [c]

[a] Laboratoire de Mécanique des Solides, École Polytechnique and CNRS, Palaiseau F-91128, France
[b] Division of Applied Science and Engineering, California Institute of Technology, Pasadena, California, USA
[c] School of Engineering and Applied Sciences, Harvard University, Cambridge, MA 02138, USA

ABSTRACT

This paper presents an asymptotically rigorous one-dimensional analytical formulation capable of accurately capturing the stress and strain distributions that develop within the evolving neck of bars and sheets of rate-dependent materials stretched in tension. The work is an extension of an earlier study by the authors on necking instabilities in rate-independent materials. The one-dimensional model accounts for the gradients of the stress and strain that develop as the necking instability grows. Material strain-rate dependence has a significant influence on the strain that can be imposed on a bar or sheet before necking becomes pronounced. The formulation in this paper enables a quantitative assessment of the interplay in necking retardation due to rate-dependence and that due to the development of hydrostatic tension in the neck. The connection with a much simpler long-wavelength approximation which does not account for curvature induced hydrostatic tension in the neck is also emphasized and extended.

© 2018 Elsevier Ltd. All rights reserved.

1. Introduction

The ability to analyze necking instabilities is central to a number of technologies. To extract stress-strain data from a tensile test of a round bar beyond the onset of necking, one must account for the non-uniform stress distribution that develops in the neck. In the shape forming of ductile sheet metals, the sheet must be stretched without incurring pronounced necking. For sufficiently ductile materials for which fracture does not precede necking, the forming limit diagrams for sheet materials display the maximum allowable in-plane stretching strains such that necking localizations remain within acceptable limits. Material strain-rate dependence is well known to play an important role in necking. For positive strain-rate hardening, which will be the focus in this paper, the rate-dependence can significantly increase the strain achievable prior to unacceptable necking localization. Raising the temperature of a metal can increase its rate-dependence and hot metal forming is a well-known means of enhancing the allowable stretching limits of bars and sheets. An extreme example is glass at elevated temperatures when its rate-dependence becomes nearly linearly viscous and a bar of the material can be stretched almost indefinitely. Rate-dependence is also frequently introduced into elastic-plastic constitutive models in finite element codes for computational reasons rather than physical fidelity and a quantitative knowledge of how this artificial rate-dependence presence affects stability phenomena is essential.

---

* Corresponding author at: Laboratoire de Mécanique des Solides, École Polytechnique and CNRS, Palaiseau F-91128, France.
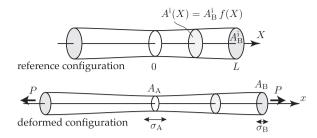*E-mail address:* audoly@lmm.jussieu.fr (B. Audoly).

Fig. 1. Analysis of a bar based on the long-wavelength approximation undeformed and deformed configurations.

The role of a positive material strain-rate dependence on retarding necking is intuitive. As the deformation begins to localize in a neck the strain-rate increases relative to the strain-rate outside the neck and this produces an additional increase of stress relative to that outside the neck. This relative local increase of stress slows the deformation in the neck relative to that outside the neck. Strain-rate hardening not only retards the grow of the neck, it also tends to spread the non-uniformity and counter localization. The strong effect of material strain-rate dependence on neck retardation will be apparent in this paper.

The effect of the non-uniform stress distribution in the neck on neck retardation is more subtle. Bridgman (1952) analyzed the stress distribution and showed that a substantial hydrostatic tension develops in the neck such that the average tensile stress supporting the load at the neck is not uniaxial but is made up of an effective stress component tied to the plastic deformation plus a contribution from hydrostatic tension. The effective Mises stress averaged across the cross-section at the center of the neck, σ_e, is reduced below the force per area at the neck, σ, thereby reducing the deformation below what would be expected for a uniform bar of the same cross-sectional area. For a round bar undergoing tensile stretching, the one-dimensional model developed by Audoly and Hutchinson (2016) for rate-independent materials includes the Bridgman effect via the ratio of the true effective stress averaged across the center of the neck to the true stress average as

$$\frac{\sigma_e}{\sigma} = \frac{1}{1 + \frac{r}{4c}} \tag{1.1}$$

where r is the current radius of the neck at its center and c is the radius of curvature of the neck in the current state at the same location given by $\frac{1}{c} = \frac{d^2 r}{dx^2}$.

The present paper extends the one-dimensional (1D) model developed by Audoly and Hutchinson (2016) to rate-dependent materials, and applies the model to necking in round bars subject to tension and to necking in thin sheet materials. The 1D model rigorously captures the lowest order influence of the non-uniformity that develops in otherwise uniformly stretched bars and sheets of rate-dependent materials. As such, it includes both the influence of the material rate-dependence and the Bridgman effect on necking localizations. Earlier work on necking in rate-dependent materials by Marciniak et al. (1973), Ghosh (1977), Hutchinson and Neale (1977), and Hutchinson et al. (1978a) has been based on a long-wavelength approximation which does not account for the Bridgman effect. Section 2 introduces the long-wavelength approximation and provides some earlier results based on this approximation as a background to the present study. The analysis leading to the 1D gradient model is given in Appendix B and in Appendix D, but a brief synopsis of the formulation for round bars and stretched sheets is given in Section 3, followed in Section 4 by its application to neck development for a class of rate-dependent materials. Section 5 presents a parallel treatment of necking in rate-dependent sheets. Conclusions are summarized in Section 6.

2. Summary of the long-wavelength approximation and results for round bars in tension

The long wavelength approximation for a round bar subject to tension assumes that the stress state at every cross-section in the bar is uniaxial tension σ with no variation across the radius, accompanied by a strain-rate that is uniform across the cross-section. The connection between the true stresses, σ_A and σ_B, and cross-sectional areas, A_A and A_B, in the current state at any two cross-sections, A and B, is

$$\sigma_A A_A = \sigma_B A_B = P \tag{2.1}$$

where P is the tensile force carried by the bar, see Fig. 1.

For rate-dependent materials necking only occurs if there is some initial non-uniformity. Departure from uniformity in the form of a bifurcation can occur for rate-independent materials but not rate-dependent materials. For the case of an initial variation of the cross-sectional area along the bar we will consistently identify A_B^i with the greatest initial area. With X as the axial coordinate along the center of the bar identifying material points in the undeformed state, the variation of the initial cross-sectional area is taken to be
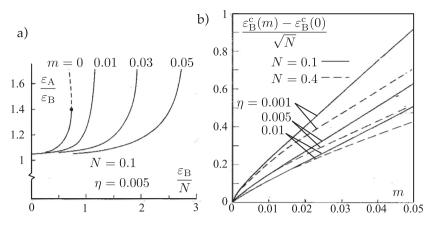
$$A^i(X) = A_B^i f(X). \tag{2.2}$$

Fig. 2. Behavior as predicted by the long-wavelength approximation. (a) With A at the center of the neck and B at the thick end of the bar, the strain ratio, $\varepsilon_A/\varepsilon_B$, is plotted as a function of ε_B/N for $N = 0.1$ and several strain-rate indices m, including the rate-independent limit $m = 0$. The initial imperfection is (2.3) with $\eta = 0.005$. (b) The normalized necking retardation, $\left(\varepsilon_B^c(m) - \varepsilon_B^c(0)\right)/\sqrt{N}$, at the necking limit due to material rate-dependence. Derived from figures in Hutchinson and Neale (1977).

A specific initial imperfection taken for some of the numerical examples is

$$f(X) = 1 - \eta\frac{1 + \cos\frac{\pi X}{L}}{2}, \tag{2.3}$$

where $\eta > 0$ is the imperfection amplitude measuring the fractional reduction in initial cross-sectional area at the minimum section and L is the initial half-length of the bar. The maximum cross-sectional area, A_B^i, is at $X = \pm L$ and the minimum, A_A^i, is at $X = 0$ with $A_A^i = A_B^i(1 - \eta)$. For this choice, the bar is symmetric with initial length $2L$. The neck will develop at the center of the bar at $X = 0$.

The uniaxial rate-dependent constitutive law employed in this study will be

$$\sigma = \sigma_R\varepsilon^N(\dot{\varepsilon}/\dot{\varepsilon}_R)^m, \text{ or } \sigma = K\varepsilon^N\dot{\varepsilon}^m \text{ with } K = \sigma_R/\dot{\varepsilon}_R{}^m. \tag{2.4}$$

where σ is the true stress, ε is the logarithmic strain and $\dot{\varepsilon}$ its time rate. The strain hardening index is N, the strain-rate hardening index is m with σ_R and $\dot{\varepsilon}_R$ as the reference stress and strain-rate, respectively. The material is assumed to be incompressible and elastic strains are neglected.

Under the assumptions stated above for the long wavelength approximation and under the assumption of incompressibility, the cross-sectional area at any section is related to the current strain ε at that section by $A = A^i e^{-\varepsilon}$. Consequently, the long wavelength approximation governing the strain-rate distribution for round bars of the material (2.4) can be written in terms of the strain-rate at section B as

$$e^{-\varepsilon/m}\varepsilon^{N/m}\dot{\varepsilon} = f(X)^{-1/m}e^{-\varepsilon_B/m}\varepsilon_B{}^{N/m}\dot{\varepsilon}_B, \tag{2.5}$$

where ε and $\dot{\varepsilon}$ denote the strain and strain-rate at a generic cross-section having coordinate X. The lack of any dependence of this governing equation on K or the reference stress and reference strain-rate is a consequence of the homogeneous dependence of the constitutive model (2.4) on the strain and strain-rate. While the necking strains depend strongly on the material index of rate-dependence m, they are independent of the reference strain-rate $\dot{\varepsilon}_R$, the reference stress σ_R and the overall rate of straining of the specimen. With L_{def} as the half-length of the deformed bar, the elongation of the bar in the long wavelength approximation is

$$\frac{L_{\text{def}} - L}{L} = \frac{1}{L}\int_0^L (e^{-\varepsilon(X)} - 1)dX. \tag{2.6}$$

For reference it is useful to begin by presenting results from Hutchinson and Neale (1977) for the long wavelength approximation in the limit of rate-independent power-law materials $m \to 0$ for which (2.5) becomes $e^{-\varepsilon/N}\varepsilon = f(X)^{-1/N}e^{-\varepsilon_B/N}\varepsilon_B$. Denote the strain at the center of the incipient neck at $X = 0$ by ε_A. As illustrated in Fig. 2a for the curve with $m = 0$, the ratio $\varepsilon_A/\varepsilon_B$ attains a vertical slope such that $d\varepsilon_A/d\varepsilon_B = \varepsilon_A/\varepsilon_B = \infty$. With this condition identified as the critical necking event, denote the associated strain at B by ε_B^c. This strain is representative of the strain attainable outside the neck. It satisfies

$$\left(\frac{\varepsilon_B^c}{N} - 1\right)\ln\frac{\varepsilon_B^c}{N} = -\frac{1}{N}\ln(1 - \eta). \tag{2.7}$$

For sufficiently small imperfections ε_B^c is given by the asymptotic formula

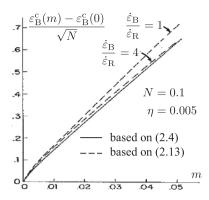$$\frac{\varepsilon_B^c}{N} \approx 1 - \sqrt{\frac{2\eta}{N}} \tag{2.8}$$

Fig. 3. Neck retardation due to material rate-dependence predicted using the long wavelength approximation for two tensile constitutive models, (2.4) and (2.13). The results for model (2.4) are independent of the imposed strain-rate, whereas those for model (2.13) have the relatively weak dependence on the imposed rate shown.

which agrees with the well-known result attributed to Considère in the limit of initially uniform bars, $\eta = 0$ and $\varepsilon_B^c = N$. The square-root in the right-hand side reflects the strong imperfection-sensitivity of necking.

For the rate-dependent material, the relation between ε_A^c and ε_B^c from (2.5) is

$$\int_0^{\varepsilon_A} e^{-\varepsilon/m} \varepsilon^{N/m} d\varepsilon = (1-\eta)^{-1/m} \int_0^{\varepsilon_B} e^{-\varepsilon/m} \varepsilon^{N/m} d\varepsilon. \tag{2.9}$$

As seen in Fig. 2a, $\varepsilon_A/\varepsilon_B \to \infty$ at a finite ε_B if $m > 0$. Denoting this value by $\varepsilon_B^c(m)$, Hutchinson and Neale (1977) have presented both numerical results and asymptotic formulas for the strain at necking. The large necking retardation due to material rate-dependence is captured by the difference, $\varepsilon_B^c(m) - \varepsilon_B^c(0)$, between the necking strain with $m > 0$ and that with $m = 0$, which is plotted for a wide range of the relevant parameters in Fig. 2b. These results for $N = 0.1$ and 0.4 were computed numerically using (2.9). The normalization of the retardation by $\sqrt{N}$ in Fig. 2b was suggested by the asymptotic formula valid for very small m:

$$\frac{\varepsilon_B^c(m) - \varepsilon_B^c(0)}{\sqrt{N}} \approx \frac{m}{2\sqrt{2\eta}} \ln \frac{4\pi\eta}{m}. \tag{2.10}$$

As is evident in Fig. 2, neck retardation due to rate-dependence is substantial. Even for m as small as 0.001, neck retardation is non-negligible.

It is worth recording that for $N = 0$ the strain and stretch at B associated with $\dot{\varepsilon}_A/\dot{\varepsilon}_B \to \infty$ according to the long wavelength approximation can be obtained analytically as

$$\varepsilon_B^c(m) = -m \ln(1 - (1-\eta)^{1/m}) \quad \text{and} \quad \lambda_B^c(m) = e^{\varepsilon_B^c} = (1 - (1-\eta)^{1/m})^{-m} \tag{2.11}$$

Furthermore, the associated distribution and average stretch at necking are

$$\begin{aligned} \lambda^c(X) &= \left(1 - \left(\frac{f(0)}{f(X)}\right)^{1/m}\right)^{-m} \\ \lambda_{ave}^c &= \int_0^1 \left(1 - \left(\frac{1-\eta}{1-\frac{\eta}{2}(1+\cos\pi z)}\right)^{1/m}\right)^{-m} dz \end{aligned} \tag{2.12}$$

where the average stretch at necking according to this model with imperfection shape (2.3) is seen to be independent of *L*.

Another tensile constitutive model considered by Ghosh (1977) for rate-dependent materials is

$$\sigma = \sigma_R \times \left(\varepsilon^N + m \ln \frac{\dot{\varepsilon}}{\dot{\varepsilon}_R}\right) \tag{2.13}$$

This relation is not homogeneous in the strain-rate and, thus, the ratio of the imposed strain rate to the reference strain-rate $\dot{\varepsilon}_R$ does play a role. The equation governing the long wavelength approximation for this relation is given by Hutchinson and Neale (1977) and their numerical analysis of neck retardation produced the comparison for the two constitutive models shown in Fig. 3. For relatively small changes in the imposed strain-rate, i.e., $\dot{\varepsilon}_B/\dot{\varepsilon}_R$ increasing from 1 to 4 in Fig. 3, the change in necking strain is relatively small and the predictions are similar to those from the pure-power constitutive model.

The homogeneous nature of the constitutive model (2.4) and the consequent independence of the relevant predictions for necking strains and elongation on the imposed strain-rate make the pure-power law model attractive for the present study, and henceforth we will employ (2.4). It can be mentioned in passing that the widely used tensile constitutive model by Johnson and Cook (1985) for behavior in the range of high strain-rates incorporates the same functional dependence on the strain-rate as that in (2.13). That law is often applied to dynamic problems in which very large strain-rates occur. The present necking study does not take into account inertial effects or nor does it address material models applicable at very high strain-rates, although we believe further extension of the 1D reduction has promise for such applications.

3. Quick presentation of the one-dimensional model

In this section, we present a summary of the 1D model governing necking of a bar (Section 3.2) or a sheet (Section 3.3) of a rate-dependent material, as derived by dimension reduction in Appendix B and Appendix D.

3.1. Three-dimensional visco-plastic model (flow theory)

The starting point of the dimension reduction for a bar or a sheet is a 3D visco-plastic model, which is formulated as follows. In terms of the Eulerian strain rate $\dot{\underline{\underline{\varepsilon}}}$, the equivalent (viscoplastic) strain rate reads

$$\dot{\varepsilon}_e = \sqrt{\tfrac{2}{3}} \, \|\dot{\underline{\underline{\varepsilon}}}\|, \tag{3.1}$$

where $\|\underline{\underline{d}}\| = \sqrt{\underline{\underline{d}} : \underline{\underline{d}}}$ denotes the Euclidean norm of a tensor $\underline{\underline{d}}$, and double underlines denote tensors. The cumulated equivalent strain is obtained by time integration as

$$\varepsilon_e = \int_0^t \dot{\varepsilon}_e \, dt'. \tag{3.2}$$

The material is assumed to be incompressible, and so

$$\operatorname{tr} \dot{\underline{\underline{\varepsilon}}} = 0. \tag{3.3}$$

The visco-plastic constitutive law is introduced by means of a potential depending on the cumulated equivalent strain ε_e and on the strain rate $\dot{\underline{\underline{\varepsilon}}}$ as

$$\Phi_{\varepsilon_e}(\dot{\underline{\underline{\varepsilon}}}) = \iiint W_{\varepsilon_e}(\dot{\varepsilon}_e) \, dx dy dz, \tag{3.4}$$

where $dx dy dz$ is the volume element. In most application examples, we will consider the power-law potential

$$W_{\varepsilon_e}(\dot{\varepsilon}_e) = K \varepsilon_e{}^N \frac{\dot{\varepsilon}_e{}^{m+1}}{m+1}, \tag{3.5}$$

where K is a modulus, see (2.4).

In all our examples, the visco-plastic flow is caused by some displacement imposed at the boundary, and there is no applied force. At any given time, the instantaneous velocity $\underline{v}$ can be found by the following variational principle: (*i*) $\underline{v}$ is isochoric and compatible with the imposed displacements, and (*ii*) with $\dot{\underline{\underline{\varepsilon}}} = (\underline{\nabla} \underline{v} + (\underline{\nabla} \underline{v})^T)/2$, $\underline{v}$ makes the potential $\Phi_{\varepsilon_e}(\dot{\underline{\underline{\varepsilon}}})$ stationary with respect to arbitrary, divergenceless velocity perturbations $\hat{\underline{v}}$ subject to the constraint $\hat{\underline{v}} = \underline{0}$ wherever the displacement is imposed.

As shown in Appendix A, this variational formulation is equivalent to the local constitutive law

$$\begin{aligned} \underline{\underline{s}} &= \tfrac{2}{3} \tfrac{\sigma_e}{\dot{\varepsilon}_e} \dot{\underline{\underline{\varepsilon}}} \\ \sigma_e &= \frac{\partial W_{\varepsilon_e}}{\partial \dot{\varepsilon}_e}(\dot{\varepsilon}_e) \end{aligned}, \tag{3.6}$$

where $\underline{\underline{s}} = \underline{\underline{\sigma}} - \underline{\underline{I}} \operatorname{tr} \underline{\underline{\sigma}}/3$ is the deviatoric part of the Cauchy stress $\underline{\underline{\sigma}}$, $\underline{\underline{I}}$ denotes the 3×3 identity matrix, and σ_e is called the equivalent strain. In an incompressible material, the Cauchy stress is defined up to a hydrostatic pressure. Note that with the help of (3.1) we have $\|\underline{\underline{s}}\| = \sqrt{\tfrac{2}{3}} \sigma_e$: this is consistent with loading in simple tension, whereby $\underline{\underline{s}} = \begin{pmatrix} 2/3 & & \\ & -1/3 & \\ & & -1/3 \end{pmatrix} \sigma_e$. Also, note that the incompressibility (3.3) and the constitutive law (3.6) warrant $\operatorname{tr} \underline{\underline{s}} = 0$.

For the particular dissipation potential in (3.5) for example, the equivalent stress reads

$$\sigma_e = K \varepsilon_e{}^N \dot{\varepsilon}_e{}^m. \tag{3.7}$$

When the long-wavelength approximation is applicable, the quantities σ_e, ε_e and $\dot{\varepsilon}_e$ can be identified with those denoted earlier as σ, ε and $\dot{\varepsilon}$, and Eq. (2.4) is recovered.

3.2. One-dimensional model for a visco-plastic cylinder

Consider a cylinder with length $2L$, and let X denote the axial coordinate in reference configuration, $-L \leq X \leq L$. Small initial imperfections are considered: the largest initial radius R is attained at the terminal cross-sections, $X = \pm L$. In the interior of the bar, the initial radius is denoted by $R^i(X) = R\sqrt{f(X)}$, where $f(X)$ is the initial *areal* imperfection factor.

The visco-plastic cylinder is deformed by the application of a time-dependent displacement at the terminal cross-sections. We use a Lagrangian representation and seek the coordinate $\Lambda(X, t)$ at time t of the cross-section initially located at position X, see Fig. 4a. The cross-sections do not remain planar upon deformation, and $\Lambda(X, t)$ is more accurately defined as the coordinate of the center of mass of the deformed cross-section whose initial coordinate was X.
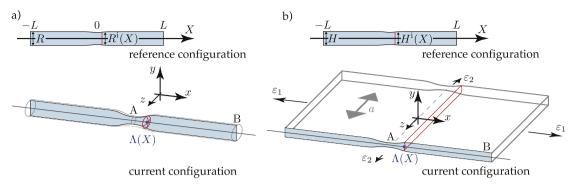
Fig. 4. One-dimensional model for (a) a cylinder and (b) and sheet necking in plane-strain.

The detailed dimensional reduction is carried out in Appendix B and Appendix D. It proceeds by assuming that the scales are separated, $R \ll L$, and that $\Lambda(X, t)$ is a slow function of X, *i.e.,* that its gradient $\partial\Lambda/\partial X$ is of order Λ/L, which is much smaller that Λ/R. Based on this assumption, the visco-plastic problem is solved order by order with respect to the small parameter R/L. In particular the full three-dimensional displacement can be determined, and it is found that the curvature of the cross-sections must be taken into account. As a result, the axial stretch averaged over a cross-section, which we refer to as the *effective stretch* and denote as $\lambda_e(X)$, is different from the gradient $\lambda(X) = \frac{\partial\Lambda}{\partial X}$ of the mean *axial* displacement; the difference is a small correction, of relative importance $(R/L)^2$, but it plays an important role. The detailed calculation for a cylinder is given in Appendix B, and yields the effective stretch as

$$\lambda_e(X, t) = \lambda(X, t) + R^2 f(X) \frac{\lambda'^2(X, t)}{16\,\lambda^4(X, t)}, \tag{3.8}$$

when higher-order corrections, of order $(R/L)^4$, are neglected, see Eq. (B.14). The dominant contribution, denoted by λ (without any subscript) is the gradient of the mean displacement,

$$\lambda(X, t) = \frac{\partial\Lambda}{\partial X}(X, t). \tag{3.9}$$

The correction proportional to R^2 in (3.8) captures the stretching of material filaments initially parallel to the axis, due to the axial gradient of transverse displacement arising from the non-uniform contraction of cross-sections, by Poisson's effect. This correction introduces a dependence on the second gradient of the displacement $\lambda'(X) = \frac{\partial\lambda}{\partial X}$, and tends to spread out the localized neck and to delay necking, as explained in the introduction. This important term is retained in the dimension reduction.

The cross-sectional average of the equivalent strain rate $\dot\varepsilon_e$ is simply denoted by $\dot\varepsilon_e(X, t)$. The dimension reduction yields a simple expression for $\dot\varepsilon_e$ in terms of the *effective* stretch λ_e, namely

$$\dot\varepsilon_e(X, t) = \frac{1}{\lambda_e(X, t)} \frac{\partial\lambda_e}{\partial t}(X, t). \tag{3.10}$$

The cross-sectional average of the cumulated equivalent strain follows by time integration as

$$\varepsilon_e(X, t) = \ln\lambda_e(X, t). \tag{3.11}$$

Finally, the dimensional reduction shows that the evolution of the one-dimensional model is governed by the effective one-dimensional visco-plastic potential

$$\Phi_\lambda(\dot\lambda) = \int_0^L \pi R^2 f(X) W_{\varepsilon_e}(\dot\varepsilon_e)\, dX. \tag{3.12}$$

In the integrand, the prefactor $\pi R^2 f(X) = \pi\left(R^i(X)\right)^2$ is the area of the undeformed cross-section, so that $\pi R^2 f dX$ is the elementary volume (which is identical in the reference and current configurations, due to incompressibility). In (3.12), the right-hand side is a function of λ, $\dot\lambda$ and their spatial gradients through the quantities $\varepsilon_e(X, t)$ and $\dot\varepsilon_e(X, t)$, see Eqs. (3.8)–(3.11).

3.3. One-dimensional model for a visco-plastic sheet in plane strain

The case of a sheet subject to a time-dependent, uniform stretch $a(t)$ in the transverse direction is shown in Fig. 4b. The imperfection is introduced by taking the initial local thickness of the plate to be $H^i(X) = Hf(X)$ where H is the maximum thickness, far from the imperfection, and $f(X) \approx 1$ defines the imperfection profile.

The detailed analysis in the appendix yields the expressions of the effective stretch as

$$\lambda_e(X, t) = \lambda(X, t) + H^2 f^2(X) \frac{\lambda'^2(X, t)}{24 a^2(t) \lambda^5(X, t)},$$ (3.13)

and of the average of the effective strain-rate over a cross-section as

$$\dot{\varepsilon}_e(X, t) = \left(\frac{4}{3} \left[\left(\frac{\dot{\lambda}_e}{\lambda_e} \right)^2 + \frac{\dot{\lambda}_e}{\lambda_e} \frac{\dot{a}}{a} + \left(\frac{\dot{a}}{a} \right)^2 \right] \right)^{1/2},$$ (3.14)

see Eqs. (D.2) and (D.3) in the Appendix. In this geometry, the determination of the cumulated elastic strain requires a time integration from (3.2), which cannot be done analytically,

$$\varepsilon_e(X, t) = \int_0^t \dot{\varepsilon}_e(X, t') \mathrm{d}t'.$$

The one-dimensional dissipation potential reads, as earlier,

$$\Phi_\lambda(\dot{\lambda}) = \int_0^L H D f(X) W_{\varepsilon_e}(\dot{\varepsilon}_e) \, \mathrm{d}X,$$ (3.15)

where D is the initial width of the plate, and the coefficient $[HDf(X)]$ is the unformed area of a cross-section of the sheet.

4. Neck retardation in bars under tension based on the 1D gradient model

Bars with circular cross-section with initial radius distribution $R^i(X)$ are considered where the initial imperfection has the form described in Section 2, such that the initial area distribution is (2.2), i.e., $\left(\frac{R^i(X)}{R} \right)^2 = f(X)$, with the minimum radius at $X = 0$ and the maximum radius, $R = R^i(L)$ at $X = L$, such that $f(L) = 1$. As has been seen in the examples in the previous section $f(X)$ is slowly varying and its minimum value $f(0)$ is only slightly less than 1. From this point on in this section, the dimensionless coordinate X/R will be denoted by X and the dimensionless half-length L/R denoted by L in the equations. The ratios of the dimensional quantities will be retained in the figures.

The effective stretch and effective logarithmic strain in the 1D model for the round bar are, from (3.8),

$$\lambda_e = \lambda + \frac{f(X)}{16} \frac{\lambda'^2}{\lambda^4} \quad \text{and} \quad \varepsilon_e = \ln \lambda_e,$$ (4.1)

with $\lambda' = \frac{\mathrm{d}\lambda}{\mathrm{d}X}$. It can be noted that $f(X)$ in (4.1) can be replaced by 1 with virtually no effect on any of the results generated in this paper, but continuing with (4.1) as it stands creates no difficulty for our solution method, so we will continue with this form. The effective stretch-rate and strain rate are

$$\dot{\lambda}_e = \left(1 - \frac{f(X)}{4} \frac{\lambda'^2}{\lambda^5} \right) \dot{\lambda} + \frac{f(X)}{8} \frac{\lambda' \dot{\lambda}'}{\lambda^4} \quad \text{and} \quad \dot{\varepsilon}_e = \frac{\dot{\lambda}_e}{\lambda_e}.$$ (4.2)

In the current state with $\lambda(X)$ known, increments of elongation are prescribed by imposing the average stretch rate $\dot{\lambda}_{ave}$ where

$$\dot{\lambda}_{ave} = \frac{1}{L} \int_0^L \dot{\lambda}(X) \, \mathrm{d}X.$$ (4.3)

The dimensional stress potential is denoted by $\sigma_R \dot{\varepsilon}_R W(\lambda_e, \dot{\lambda}_e)$ such that

$$\sigma = \sigma_R \dot{\varepsilon}_R \frac{\partial W}{\partial \dot{\varepsilon}_e} = \sigma_R \dot{\varepsilon}_R \lambda_e \frac{\partial W}{\partial \dot{\lambda}_e}.$$ (4.4)

The dimensionless functional whose first variation generates the solution for the rate problem is

$$\Phi(\dot{\lambda}) = \int_0^L f(X) W(\lambda_e, \dot{\lambda}_e) \mathrm{d}X - \zeta \left[\frac{1}{L} \int_0^L \dot{\lambda}(X) \mathrm{d}X - \dot{\lambda}_{ave} \right],$$ (4.5)

where ζ is a Lagrangian multiplier. The stretch-rates have $\dot{\lambda}' = 0$ at $X = 0, L$ for the imperfection (2.3). If the gradient terms in λ_e and $\dot{\lambda}_e$ are deleted, this variational principle delivers the long wavelength approximation.

As previously noted in (3.5), the tensile constitutive law (2.4) is represented by the potential

$$W = \frac{1}{m+1} \varepsilon_e^{\ N} \left(\frac{\dot{\varepsilon}_e}{\dot{\varepsilon}_R} \right)^{m+1}$$ (4.6)

while the imperfection profile is chosen as $f(X) = 1 - \frac{\eta}{2} \left(1 + \cos \frac{\pi X}{L} \right)$. The numerical method based on (4.5) is discussed in Appendix E.
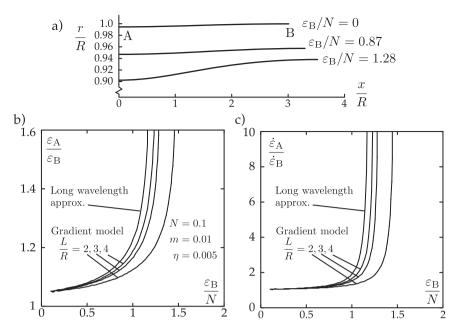
Fig. 5. Necking of a bar based on the 1D gradient model and comparison to the long wavelength approximations. (a) Deformed shapes predicted by the 1D gradient model for $L/R = 3$. The evolution of the strain ratio, $\varepsilon_A/\varepsilon_B$, is plotted in (b) and the strain-rate ratio, $\dot{\varepsilon}_A/\dot{\varepsilon}_B$, is plotted in (c) as a function of ε_B/N.
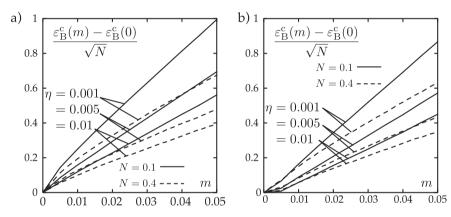

Fig. 6. Neck retardation due to material strain-rate dependence as predicted by the 1D model for $L/R = 2$ in part (a) and for $L/R = 4$ in part (b). The necking condition is taken to be $\dot{\varepsilon}_A/\dot{\varepsilon}_B = 5$. These plots can be compared with the corresponding plot based on the long wavelength approximation in Fig. 2b which does not depend on L/R.

Fig. 5 presents representative results for the evolution of the ratios, $\varepsilon_A/\varepsilon_B$ and $\dot{\varepsilon}_A/\dot{\varepsilon}_B$, of the strain and strain-rate at the center of the neck to the corresponding values at the end of the bar where it is the thickest. These have been computed using the 1D gradient model with $N = 0.1$, $m = 0.01$ and $\eta = 0.005$ for three values of L (e.g., L/R in terms of dimensional quantities). Included in the plots are the predictions based on the long wavelength approximation introduced earlier which does not depend on L. The horizontal axis is ε_B/N which would attain a maximum value of unity with no strain-rate dependence, $m = 0$, and no imperfection, $\eta = 0$. The shape of the bar is also shown for the case $L = 3$ at three values of ε_B/N. As discussed in the Introduction, the Bridgman effect, whereby the effective stress is reduced in the neck due to the developing hydrostatic tension, contributes to neck retardation. This effect is more pronounced the higher the gradients, i.e., the smaller is L in Fig. 5. Bars having imperfections with $L = 4$ or larger are well represented by the long-wavelength approximation.

For the gradient model, which is solved numerically, we take the necking condition to be $\dot{\varepsilon}_A/\dot{\varepsilon}_B = 5$ which, as seen in Fig. 5, means the associated strain ε_B^c will be slightly less than that associated with $\dot{\varepsilon}_A/\dot{\varepsilon}_B \to \infty$. Recall that $\dot{\varepsilon}_A/\dot{\varepsilon}_B \to \infty$ was adopted as the necking criterion in computing the results in Figs. 2 and 3 based on the long wavelength approximation. The difference between the strain outside the neck for the two choices defining necking, which is the primary quantity of interest, is only a couple of percent. Plots of the neck retardation due to the material strain-rate behavior as predicted by the gradient model are shown in Fig. 6a and b for $L = 2$ and 4. These plots can be compared with the corresponding results
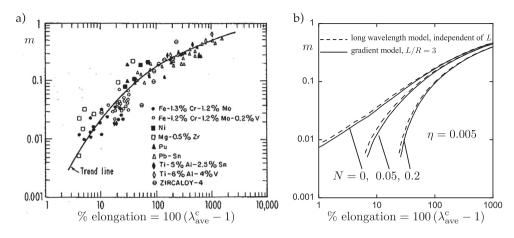
Fig. 7. Percentage elongation at necking as dependent on material strain-rate dependence. (a) Data from Woodford (1969) for a collection of metals. (b) Predictions from the 1D gradient model for three values of N for $\eta = 0.005$ with $L/R = 3$ and from the long wavelength model, both based on the assumption that necking coincides with the attainment of $\dot{\varepsilon}_A / \dot{\varepsilon}_B = 5$.

for the long wavelength model in Fig. 2b which do not depend on L. It is clear from Figs. 5 and 6, and those to follow, that the material rate-dependence as characterized by m plays the dominant role in retarding necking. The Bridgman effect further retards necking but only as a secondary effect. The material rate-dependence slows the localization of an initially broad imperfection thereby delaying the development of the Bridgman effect. An important implication of this observation is that the long-wavelength approximation is reasonably accurate for materials with significant positive rate-dependence.

Woodford (1969) has collected the elongation data for the a large set of metals having a wide range of strain-rate dependence and plotted the percentage elongation as it depends on m. Woodford's plot is reproduced in Fig. 7a. Predictions from the long wavelength model which for the imperfection shape (2.3) are independent of L and from 1D gradient model with $L = 3$ are presented in Fig. 7b for three values of N.

We proceed to analyze initial imperfections having a short wavelength: they enhance the gradient effects as we show now. Initial imperfections with widths on the order of the diameter of the round bar can be expected under certain circumstances. While it might seem that such wavelengths push the limits of validity of the asymptotic 1D reduction, earlier work on rate-independent necking by Audoly and Hutchinson (2016) has shown that the reduction retains accuracy to such short wavelengths as long as the necking amplitude is moderate. For this purpose 'localized' imperfections are considered of the form

$$A^i(X) = \pi R^2 \left(1 - \eta \frac{e^{-(X/\ell)^2} - e^{-(L/\ell)^2}}{1 - e^{-(L/\ell)^2}} \right) \equiv \pi R^2 f(X) \tag{4.7}$$

with ℓ on the order of R. As earlier, the maximum area is $A^i_B \equiv A^i(L) = \pi R^2$. For long bars having $L/\ell \gg 1$, $f(X) = 1 - \eta e^{-(X/\ell)^2}$.

Denote the deficit in cross-sectional area at the center of the neck relative to that well outside the neck normalized by the area well outside the neck by $[(A_B)_{\text{def}} - (A_A)_{\text{def}}]/(A_B)_{\text{def}}$ with $(A_A)_{\text{def}}$ and $(A_B)_{\text{def}}$ as the respective areas in the deformed state. Noting that this normalized deficit is the imperfection amplitude η in the initial state, the measure $[(A_B)_{\text{def}} - (A_A)_{\text{def}}]/[\eta (A_B)_{\text{def}}]$ provides the growth of the neck in multiples of the initial imperfection amplitude. Fig. 8 presents plots of ε_B/N versus this measure for two values of imperfection wavelength computed using the 1D reduction for an intermediate value of the strain-rate hardening index $m = 0.1$, $N = 0.2$ and $\eta = 0.005$. Measured in multiples of the imperfection amplitude, the trends are only weakly dependent on the amplitude itself, as will be seen later when thin sheet necking is discussed. The role of gradient effects via the dimensionless imperfection width parameter ℓ/R is also revealed. Included in Fig. 8 are predictions based on a modification of the long-wavelength approximation that includes the lowest order influence of the stretch gradient. This modification is derived from the 1D reduction in Appendix F. With $\lambda(X) = \lambda_B + \eta \Delta\lambda(X)$ as the stretch, the resulting equation for the stretch-rate in the modification of the long-wavelength approximation for the round bar is

$$\Delta\dot{\lambda} = \frac{1}{\eta} \left\{ \left(1 + \frac{\eta \Delta\lambda}{\lambda_B} \right) \left[\frac{1}{f(X)} \left(1 + \eta \frac{\Delta\lambda}{\lambda_B} \right) \left(\frac{\varepsilon_e^B}{\varepsilon_e} \right)^N \left(1 + \frac{\eta \Delta\lambda''}{8\lambda_B^4} \right)^{1/m} - 1 \right] \right\} \dot{\lambda}_B. \tag{4.8}$$

This result reduces precisely to the long-wavelength approximation if the term involving $\Delta\lambda''$ is deleted. In Fig. 8 it can be noted that this simple extension captures the gradient effects on necking retardation fairly accurately to values of the normalized area deficit of thirty times the initial imperfection amplitude. Further discussion of implementing the extension is given in Appendix F.
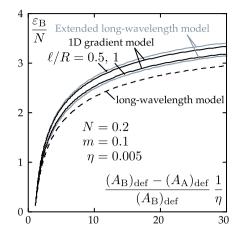
Fig. 8. Normalized strain attainable outside the neck as dependent on the thickness deficit at the center of the neck relative to the thickness outside the neck expressed in multiples of the initial deficit, η, for the *local* imperfection (4.7). Plotted for $\eta = 0.005$ based on both the long-wavelength approximation and the gradient model for two values of the imperfection width parameter ℓ/R. The corresponding curves based on the simple approximation in Eq. (4.8) accounting for the lowest order influence of the gradient are also shown. The choice of L/R is large enough such that it has no influence on the results.

If instead of initial geometric imperfections in the form of (2.3) or (4.7) one considered a geometrically perfect round bar which had a slightly non-uniform variation in the reference yield stress according to $\sigma_R(X) = \sigma_R^B f(X)$, then the problem for the evolving strain distribution would again be governed by the incremental boundary value problem derived from (4.5), the only exception being that $f(X)$ must be replaced by unity in Eqs. (4.1) and (4.2). For the small imperfections considered in this paper (*i.e.*, $\eta \leq 0.01$) this replacement has a negligible influence on the predictions, as has been verified by direct numerical simulations. Thus, all the results in Sections 2 and 4 apply to both initial geometric imperfections and reference stress imperfections with the same distribution $f(X)$.

5. Neck retardation in sheets based on the 1D gradient model

A forming limit diagram provides the limits to which a metal sheet can undergo in-plane biaxial stretch without developing noticeable necking or failure due to fracture. The M.-K. model of Marciniak et al. (1973) for predicting forming limit diagrams is a long-wavelength model which tracks the growth of strain in an initial imperfection band of slightly reduced thickness relative to the strain in the sheet outside the band. Uniform biaxial stretching is imposed on the sheet outside the band. Here, we focus on deformation, not material fracture, and extend the M.-K. model by applying the 1D gradient model to study neck development in sheets of rate-dependent materials stretched under conditions of in-plane plane strain. We will also digress briefly to discuss challenges that remain to be overcome with regard to fundamental plasticity theory developments before the gradient model can be extended to reliably predict sheet necking under general biaxial stretching.

5.1. Geometry of the sheet

The initial imperfection is a slight thickness reduction of the sheet taken in the form of a straight band oriented perpendicular to the direction of maximum principal strain ε_1, see Fig. 4b. We will focus on the case where the sheet is constrained such that the strain parallel to the band is zero, *i.e.*, $\varepsilon_2 = 0$, corresponding to plane strain: the reason for this is exposed in Section 5.2 below.

With H as the initial thickness of the sheet at the edges at $X_1 = \pm L$, the initial thickness variation in the sheet is taken to be

$$H^i(X_1) = H\left(1 - \eta\frac{e^{-(X/\ell)^2} - e^{-(L/\ell)^2}}{1 - e^{-(L/\ell)^2}}\right) \equiv Hf(X_1), \tag{5.1}$$

where X_1 is the Lagrangian coordinate in the direction of the maximum principal strain, η is the initial fractional thickness reduction at the center of the band at $X_1 = 0$ relative to that at $X_1 = \pm L$, and ℓ characterizes the half-width of the imperfection. Our primary interest will be in relatively narrow bands which are not only much smaller than the initial half-width of the sheet L, but on the order of the sheet thickness, *i.e.*, $\ell \leq H$. The question of interest is how the non-uniformity develops as the sheet is stretched due to the influence of rate-dependence and the gradient effects accounted for in the 1D model. The sheet is infinite in extent in the X_2 direction, and solutions depending only on X_1 are sought. As already noted, the sheet is constrained parallel to the band such that $\varepsilon_2 = 0$.
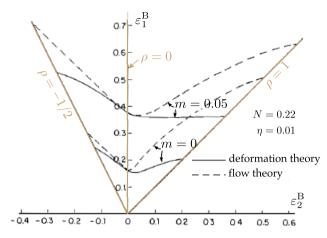
Fig. 9. Examples of forming limit diagrams predicted for the two multiaxial constitutive models (5.2) and (5.3) taken from Hutchinson et al. (1978a). The curves are based on the long-wavelength approximation for the maximum strains attained outside the neck under biaxial stretching imposed on the sheet outside the neck with $\varepsilon_2^B = \rho \varepsilon_1^B$.

5.2. Uncertainties on the constitutive model suggest limiting attention to plane-strain

In uniaxial tension, the material is assumed to obey the same constitutive relation used in the round bar analysis, *i.e.*, (2.4). Neck development and localization under biaxial stretching brings in fundamental constitutive issues that are not present for the round bar, as discussed in some detail by Stören and Rice (1975) and Hutchinson et al. (1978a,b). Here we digress briefly to review these issues as they relate to the present study. To highlight the issues we begin by listing two isotropic multi-axial constitutive models each of which reduces to (2.4) in uniaxial tension. The equations are expressed using the principal components of the true stress σ_i, the deviator stress s_i, and the logarithmic strain ε_i. In accord with Section 3.1, the equivalent stress is $\sigma_e = \sqrt{\frac{3}{2} s_i s_i} = \sqrt{\frac{3}{2} \|\underline{s}\|}$ and the material is taken to be incompressible such that $\varepsilon_1 + \varepsilon_2 + \varepsilon_3 = 0$; elastic strains are neglected. The generalization of (2.4) referred to as 'flow theory' has been presented in Section 3.1 and reads

$$\begin{cases} s_i = \frac{2}{3} K \varepsilon_e^{\,N} \dot{\varepsilon}_e^{\,m} \frac{\dot{\varepsilon}_i}{\dot{\varepsilon}_e} \\ \dot{\varepsilon}_e = \sqrt{\frac{2}{3} \dot{\varepsilon}_i \dot{\varepsilon}_i} \quad \varepsilon_e = \int \dot{\varepsilon}_e \mathrm{d}t. \end{cases} \tag{5.2}$$

The generalization of (2.4) referred to as 'deformation theory' is

$$\begin{cases} s_i = \frac{2}{3} K \varepsilon_e^{\,N} \dot{\varepsilon}_e^{\,m} \frac{\varepsilon_i}{\varepsilon_e} \\ \varepsilon_e = \sqrt{\frac{2}{3} \varepsilon_i \varepsilon_i} \quad \dot{\varepsilon}_e = \frac{\mathrm{d}\varepsilon_e}{\mathrm{d}t}. \end{cases} \tag{5.3}$$

with $K = \sigma_R / \dot{\varepsilon}_R$ in each case. Note that the definition of the equivalent strain, ε_e, is different in the two cases, and the two definitions only coincide if the strain components are increased proportionally, *i.e.*, when the strains are increased such that their ratios remain fixed. It is readily verified that both versions reduce to (2.4) in uniaxial tension and that the two versions are identical for proportional straining.

The two relations (5.2) and (5.3) can readily be implemented within the long-wavelength approximation (*i.e.*, the M.-K. model) to predict necking limits for biaxial sheet stretching. With ε_1^B and ε_2^B denoting the strains outside the band and stretching imposed such that $\varepsilon_2^B = \rho \varepsilon_1^B$ with ρ held fixed (the assumption $\rho = 0$ is relaxed temporarily and will be restored in the next section, one computes the maximum strains that can be imposed on the sheet outside the band, analogous to the necking strains computed using the long-wavelength approximation for the bar in tension. Examples of the resulting forming limit diagrams as predicted for the two constitutive models taken from Hutchinson et al. (1978a) are presented in Fig. 9 for the limit of a rate-independent material ($m = 0$) and a rate-dependent material ($m = 0.05$), for the same level of initial imperfection $\eta = 0.01$ in each case. The trend seen for the flow theory material with sharply increasing necking strains for conditions approaching equi-biaxial stretching ($\rho \approx 1$) is not in accord with experimental trends. The limitations of J_2 flow theory as applied to instability phenomena which involve strongly non-proportional straining such as sheet necking and some plastic buckling problems for plates and shells are now well known. The flow theory is based on the Mises yield surface and it is overly stiff for increments of flow that have a significant incremental strain component that is not normal to the yield surface. The classical visco-plastic flow theory (5.2) is incapable of giving physically realistic predictions for this type of plastic instability.

For rate-independent materials, Stören and Rice (1975) employed the deformation theory version, (5.3), with $m = 0$ in their bifurcation analysis of sheet necking. Their result for the strain in the uniform sheet at the onset of necking (necking

bifurcation) is

$$\varepsilon_1 = \frac{3\rho^2 + N(2+\rho)^2}{2(2+\rho)(1+\rho+\rho^2)} \quad \text{and} \quad \varepsilon_2 = \rho\varepsilon_1 \quad \text{(for } m = 0 \text{ and } \eta = 0\text{)}. \tag{5.4}$$

This result assumes that the incipient neck forms perpendicular to the direction of maximum in-plane strain which restricts application to $0 \leq \rho \leq 1$. The Stören-Rice result for $N = 0.22$ (not shown in the figure) lies above the deformation theory curve in Fig. 9 for $m = 0$ because it does not account for the reduction due to the imperfection.

The issues that stand in the way of conducting a study of biaxial stretching with $\rho \neq 0$ based on the 1D gradient model are, first, the inadequacy of the flow theory (5.2) and, second, the fact that the multi-axial deformation theory (5.3) does not admit a strain-rate potential for the stresses. To our knowledge, there does not exist a rate-dependent visco-plastic theory derived from a strain-rate potential that would relax the overly stiff incremental behavior associated with the flow theory (5.2) for non-proportional strain increments, analogous, for example, to the corner theory of Christoffersen and Hutchinson (1979) for rate-independent materials. It is likely that a weak formulation of the governing equations of the 1D gradient model employing the deformation theory (5.3) could be used to predict behavior under general biaxial stretching, but we will not pursue that option here. Another compromise would be to employ a kinematic hardening version of visco-plastic flow theory. The higher curvature of the yield surface as compared to J_2 flow theory brings the forming limit prediction more in line with the experimental observations and with the deformation theory predictions, but still with a noticeable discrepancy for realistic initial imperfections. Instead, in this paper we will limit consideration to sheet necking under conditions of in-plane plane strain with $\rho = 0$. For this case, straining is proportional throughout the sheet within the framework of the model, the two constitutive models coincide and, consequently, the necking predictions for the two constitutive models are the same, as seen for the long-wavelength approximation used in Fig. 9: in this figure, the predictions of deformation theory (solid curve) and flow theory (dashed curve) coincide along the vertical axis, $\rho = 0$.

5.3. Analysis of necking in sheets deforming in plane-strain

Dimensionless quantities are introduced in the equations which follow with $X = X_1/H$, $\ell/H \to \ell$, $L/H \to L$ and $H^i(X)/H \to H^i(X) = f(X)$. The transverse constraint requires $\varepsilon_2 = 0$ such that $\varepsilon_3 = -\varepsilon_1$. The stretch along the mid-plane of the sheet in the 1-direction is $\lambda(X) = e^{\varepsilon_1(X)}$ and $\varepsilon_1^B = \ln \lambda_B$ is the strain at $X = \pm L$. The effective strain averaged across the cross-section at X, ε_e, from the 1D gradient model is defined in (3.13) and (3.14) as:

$$\varepsilon_e(X) = \frac{2}{\sqrt{3}} \ln \lambda_e \quad \text{with} \quad \lambda_e(X) = \lambda(X) + \frac{f^2(X)\lambda'^2(X)}{24\lambda^5(X)} \tag{5.5}$$

where $\lambda' = \frac{d\lambda}{dX}$. In the general expressions of the 1D model (3.13) and (3.14), we have set the transverse macroscopic stretch as $a(t) = 1$ and $\dot{a} = 0$, consistent with the assumption $\rho = 0$, and have dropped the thickness factor H whose value is $H = 1$ in our rescalings. As in the case of the round bar, f^2 in the second term in λ_e above can be replaced by 1 for the small initial imperfections considered in the present study, as the other factor f appearing in the integrand of the potential in (3.15) has a much stronger effect.

The material strain-rate potential W used in the calculations for sheet necking is again given by (4.6) such that for prescribed average stretch increments, $\dot{\lambda}_{ave}$, the dimensionless variational principle governing the rate boundary value problem takes precisely the same form as that for the round bar in (4.5). Apart from the differences in the definitions of the effective stretch in the two problems, compare (4.1) and (5.5), the formulation for plane strain sheet necking is identical to that for necking of the round bar in tension. The same numerical method is used for generating both sets of predictions. Also, an imperfection in the form of variation of the reference stress according to $\sigma_R(X) = \sigma_R^B f(X)$ is equivalent to the initial thickness variation $H^i(X) = Hf(X)$ if one replaces f^2 by 1 in the definition of λ_e.

Figs. 10 and 11 present the deformation at the center of the neck, $X = 0$, as a function of the normalized strain well outside the neck, ε_1^B/N, for a sheet with material parameters, $N = 0.2$ and $m = 0.1$, and an initial imperfection amplitude $\eta = 0.005$. The half-length of the sheet in the 1-direction is chosen to be large enough such that these curves are independent of the aspect-ratio L/H and such that well outside the necking region the strain is essentially uniform and equal to ε_1^B. The evolving ratio of the thickness of the sheet at the center of the neck, $(H_A)_{def}$, to the thickness well outside the neck, $(H_B)_{def}$, is plotted in Figs. 10a and 11a. The ratio of the corresponding strain-rates is plotted in Figs. 10b and 11b. In Fig. 10, results are presented for different values of the rate-dependence index m, while in Fig. 11, results are presented for both the long-wavelength approximation, which is independent of the imperfection wavelength parameter, ℓ, and for the 1D gradient model for three values of ℓ/H. For $\ell/H = 1$ the gradient model predicts that the growth of the neck is only slightly more retarded than the prediction of the long-wavelength model. Moreover, for this value of the rate-dependence index, $m = 0.1$, material strain-rate effects have the dominant influence on necking retardation allowing strains outside the neck ε_1^B to attain 2 to 3 times the strain hardening index N, depending on the depth of neck that can be accepted. For imperfections with a width parameter in the range $\ell/H \leq 0.5$, the Bridgman effect captured by the gradient model does further retard neck development but this appears to be a secondary contribution when the material strain-rate dependence is appreciable.

Further insight is obtained by presenting the growth of the neck in the manner used for the round bar wherein the deficit in the thickness at the neck is employed. The normalized strain outside the neck, ε_1^B/N, is plotted in Fig. 12 as
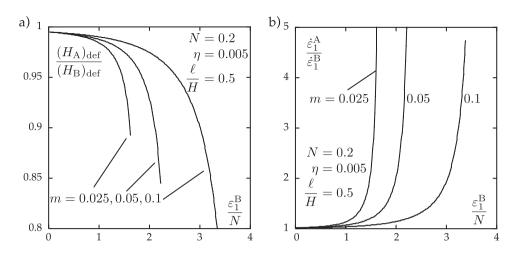
Fig. 10. Gradient model prediction of necking in a sheet. (a) Evolution of the thickness ratio of the section at the center of the neck to sections well outside the neck, $(H_A)_{def}/(H_B)_{def}$, as a function of the normalized strain well outside the neck, ε_1^B/N, for three values of the strain-rate index. (b) Evolution of the ratio of the strain-rate in the center of the neck to that well outside the neck for the same values of the strain-rate index. These have been computed with $N = 0.2$, $\eta = 0.005$, $\ell/H = 0.5$ with L/H large enough such that it has no influence on the results.
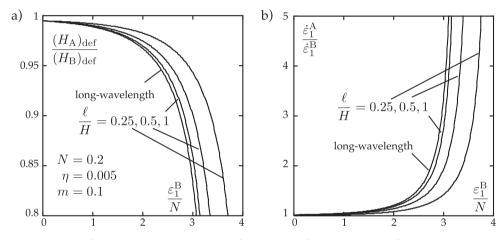

Fig. 11. Gradient model prediction of necking in a sheet. (a) Prediction of the evolution of the thickness ratio of the section at the center of the neck to sections well outside the neck, $(H_A)_{def}/(H_B)_{def}$, as a function of the normalized strain well outside the neck, ε_1^B/N, for the long-wavelength approximation and three values of the imperfection width as specified by ℓ/H. (b) Companion plots of the evolution of the ratio of the strain-rate in the center of the neck to that well outside the neck. These have been computed with $N = 0.2$, $\eta = 0.005$, $m = 0.1$ with L/H large enough such that it has no influence on the results.

a function of the relative thickness deficit normalized by η for the same cases shown in Fig. 11. The important feature revealed by this plot is that the strain that can be attained outside the neck is nearly independent of the imperfection amplitude when the relative thickness deficit is expressed as a multiple of the initial imperfection amplitude. When material strain-rate dependence is significant, the strain attainable outside the neck for realistic initial imperfection amplitudes, *i.e.,* $0.001 \leq \eta \leq 0.01$, depends mainly on the growth of the thickness deficit relative to the initial imperfect amplitude, that is, on $\frac{(H_A)_{def} - (H_B)_{def}}{\eta (H_B)_{def}}$. Fig. 12 also brings out the role of the imperfection width parameter, ℓ/H. Due to the Bridgman effect, narrower initial imperfections grow more slowly than broader ones and the effect is important if $\ell/H < 0.5$. Included in Fig. 12 are the curves computed using the extension of the long-wavelength model accounting for the lowest order influence of the gradients which is given in Appendix F. As noted for the example presented for the round bar, the simple extension of the long-wavelength model captures the gradient effect quite accurately.

The two parts of the final figure, Fig. 13, display to the extent it is possible in a single figure a summary dependence of the roles of the various dimensionless material and geometric parameters on the strain that can be imposed on the sheet under conditions of plane strain stretching. For the simulations in Fig. 13, the sheet is stretched until the difference between the thickness inside the neck to that outside the neck, normalized by the thickness outside the neck, reaches 10 times the initial imperfection amplitude. In Fig. 13a, the normalized strain ε_1^B/N at which this thickness deficit is attained is
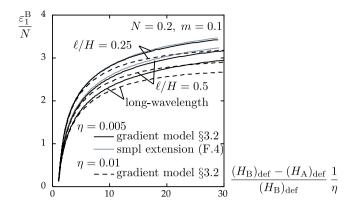
Fig. 12. Normalized strain attainable outside the neck in a sheet, as dependent on the thickness deficit at the center of the neck relative to the thickness outside the neck expressed in multiples of the initial deficit, η. Plotted for two values of η based on both the long-wavelength approximation and the gradient model for two values of the imperfection width parameter ℓ/H. The lighter curve for each of the two values of ℓ/H for $\eta = 0.005$ is the prediction of the simple approximation accounting for the lowest order influence of the gradient in Eq. (F.4). The corresponding curves for $\eta = 0.001$ are similar lying just above those for $\eta = 0.005$ but are not shown to avoid overcrowding. The choice of L/H is large enough such that it has no influence on the results.
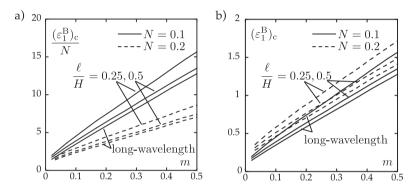

Fig. 13. Strain attained outside the neck in a sheet, as a function of the material strain-rate index m plotted using the criterion that the relative thickness deficit in the neck is 10 times the initial defect, *i.e.,* $\frac{(H_A)_{def} - (H_B)_{def}}{(H_B)_{def}} = 10\,\eta$. a) Normalized strain $(\varepsilon_1^B)_c/N$. b) Strain $(\varepsilon_1^B)_c$. Results are plotted for the long-wavelength and for the gradient model with two values of the initial imperfection width parameter. The calculation were made with $\eta = 0.005$, but the dependence on η is weak as seen in Fig. 12. The choice of L/H is large enough such that it has no influence on the results.

plotted against the rate-hardening index m, while the same results are plotted as the un-normalized strain ε_1^B in Fig. 13b, in both cases for $N = 0.1$ and 0.2. The two parts of Fig. 13 reveal that the attainable strain scales with N for $m < 0.05$, but is nevertheless significantly enhanced by the rate-dependence. For values of m greater than about 0.1, Fig. 13b reveals that the effect of N is relatively small. In this range the rate-dependence as determined by m dominates both the strain hardening N and the gradient effect as reflected by the dependence on ℓ/H.

6. Conclusions

The extension of the 1D gradient model to necking in bars and sheets has brought out the relative importance of strain-rate hardening and the Bridgman effect in neck retardation. At low levels of material rate-dependence, *i.e.,* $m < 0.01$, the tendency for the neck to localize to a width comparable to the diameter of a bar or the thickness of the sheet remains strong and both the rate-dependence and the Bridgman effect play important roles in localization and in retarding neck growth. Rate-dependence on necking is non-negligible even for values of the strain-rate hardening index as low as $m = 0.001$. This observation has implications for visco-plastic constitutive models introduced as surrogates for rate-independent material models to facilitate computations in finite element codes. If the objective is to model the development of plastic instabilities such as necks or shear bands, one must take care not to introduce material rate-dependence if it is not actually present, or to include a realistic representation when it is present, even if the level is low. When material rate-dependence is strong, *e.g.,* $m > 0.01$, it tends to dominate neck development such that the Bridgman effect becomes of secondary importance. The rate-dependence has two effects on neck growth. It retards the growth of the amplitude of the neck, and it also slows the tendency of the neck width to localize to a dimension set by the bar diameter or the sheet thickness. When material rate-dependence is significant, the relatively simple long-wavelength approximation provides a surprisingly accurate description of neck development especially if the imperfection widths are larger than the thickness of the specimen cross-section. Gra-

dient effects become more prominent for imperfections with widths that are on the order of, or less than, the specimen thickness. The simple extension of the long-wavelength approximation given in Appendix F that incorporates the lowest order contribution of the stretch gradients accurately captures the influence on neck retardation of material rate-dependence and the Bridgman effect.

Results in this paper have been obtained using the relatively simple constitutive law $\sigma = \sigma_R \varepsilon^N (\dot{\varepsilon}/\dot{\varepsilon}_R)^m$ for which the stress depends on the strain to a power and the strain-rate to another power. As a consequence of the homogeneous dependence on the strain and strain-rate, the necking strains do not depend on the reference stress σ_R or on the reference strain-rate $\dot{\varepsilon}_R$, nor do they depend on the overall rate at which the bar or sheet is stretched. For this simple model, the necking strains depend on the material parameters, N and m, and the geometric parameters specifying the imperfection, namely its dimensionless amplitude η and its shape $f(X)$ which in turn depended on a dimensionless wavelength parameter. For both the long-wavelength approximation and the 1D gradient model, the necking results based on the geometric imperfection apply equally well to an initial variation of the reference stress with dimensionless amplitude η and shape $f(X)$. Other constitutive laws can be incorporated into the 1D gradient model, usually with some sacrifice in the simplicity of the results in terms of the number of parameters on which the solutions depend. Finally, we mention again that the emphasis in this paper has been on 'slow' straining, and that inertial effects and constitutive behavior associated with high strain rates have not been considered. We hope that that the 1D model will be extended in future work to address high loading rates.

Appendix A. Variational derivation of the 3-d visco-plastic model

In this Appendix, we justify the equivalence between the formulation of the visco-plastic model based on the potential $\Phi_{\varepsilon_e}(\dot{\underline{\varepsilon}})$ introduced in Eq. (3.4), and that based on the constitutive law (3.6), as announced in Section 3.1.

The same assumptions and notations are used as in Section 3.1. We consider an incompressible visco-plastic material in 3-d, and use an Eulerian description of motion. In terms of the strain rate $\dot{\underline{\varepsilon}}$, we define the equivalent (viscoplastic) strain rate by $\dot{\varepsilon}_e = \sqrt{\frac{2}{3}} \|\dot{\underline{\varepsilon}}\|$, see (3.1) in the main text, and the cumulated equivalent strain by $\varepsilon_e = \int_0^t \dot{\varepsilon}_e \, dt'$, see (3.2). The incompressibility is expressed by $\mathrm{tr}\,\dot{\underline{\varepsilon}} = 0$, see (3.3).

The visco-plastic response is introduced by means of a potential depending on both the cumulated equivalent strain ε_e and on equivalent strain rate $\dot{\varepsilon}_e$, $\Phi_{\varepsilon_e}(\dot{\varepsilon}_e) = \iiint W_{\varepsilon_e}(\dot{\varepsilon}_e)\,dv$, see (3.4).

The variational principle stated in Section 3.1 implies that, for any virtual velocity $\hat{\underline{v}}$ which cancels on the terminal cross-sections where the displacement is applied,

$$0 = -\iiint \frac{\partial W_{\varepsilon_e}}{\partial \dot{\varepsilon}_e}\, \widehat{\dot{\varepsilon}}_e \, dx dy dz + \iiint p\,\mathrm{tr}\,\widehat{\dot{\underline{\varepsilon}}}\, dx dy dz,$$

where the first term is the variation of the potential $\Phi_{\varepsilon_e}(\dot{\varepsilon}_e)$, the second term is the Lagrange multiplier associated with the incompressibility constraint. In the first integral, we denote the partial derivative as $\sigma_e = \frac{\partial W_{\varepsilon_e}}{\partial \dot{\varepsilon}_e}$, in accord with (3.6) and the variation of the equivalent strain rate can be expressed $\widehat{\dot{\varepsilon}}_e = \sqrt{\frac{2}{3}} \frac{\dot{\underline{\varepsilon}}:\widehat{\dot{\underline{\varepsilon}}}}{\|\dot{\underline{\varepsilon}}\|} = \left(\frac{2}{3}\frac{\dot{\underline{\varepsilon}}}{\dot{\varepsilon}_e}\right):\widehat{\dot{\underline{\varepsilon}}}$. Therefore, we can rewrite the previous equations as

$$0 = -\iiint \left(\frac{2}{3}\frac{\sigma_e}{\dot{\varepsilon}_e}\dot{\underline{\varepsilon}} - p\underline{I}\right):\widehat{\dot{\underline{\varepsilon}}}\, dx dy dz$$

Identifying this expression with the principle of virtual work for a generic incompressible continuum,

$$0 = -\iiint \underline{\sigma}:\widehat{\dot{\underline{\varepsilon}}}\,dx dy dz + \iiint p\,\mathrm{tr}\,\widehat{\dot{\underline{\varepsilon}}}\,dx dy dz = -\iiint (\underline{\sigma} - p\underline{I}):\widehat{\dot{\underline{\varepsilon}}}\,dx dy dz,$$

we arrive at the expression of the Cauchy stress announced earlier in (3.6), namely $\underline{\sigma} - p\underline{I} = \underline{s} = \frac{2}{3}\frac{\sigma_e}{\dot{\varepsilon}_e}\dot{\underline{\varepsilon}}$.

Appendix B. Dimension reduction for a cylinder

In Appendix B through Appendix D, we use different notation than in the main text. This should not bring any confusion, since the only overlap between these appendices and the main text are the formulas defining the 1D model: these equations are derived in the appendices and also rewritten using the notations relevant to the main text in Section 3.

B1. Kinematic analysis of a cylinder

We consider a visco-plastic cylinder. In undeformed configuration, the cylinder radius is denoted as ρ. Let (R, Θ, X) denote the cylindrical coordinates of a material points in reference configuration, and $(\underline{e}_R(\Theta), \underline{e}_\Theta(\Theta), \underline{e}_X)$ the cylindrical basis. The coordinate X is along the axis, and is used to label material cross-sections, $0 \leq X \leq L$ where L is the undeformed length of the bar. The radial coordinate R satisfies $0 \leq R \leq \rho$: the axis is $R = 0$ and (R, Θ) are polar coordinates in the plane of the cross-section (Fig. B.14).
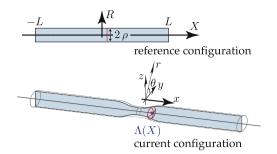
Fig. B.14. Necking of a bar: notation used in the Appendix.

We use a Lagrangian description of motion, and denote by $\underline{x}(R, \Theta, X)$ the position of a material point in deformed configuration. The dependence on time is ignored for the moment, but it will be restored later on. The cylindrical coordinates of $\underline{x}$ are denoted by (r, θ, x). We assume that cylindrical invariance is preserved upon deformation,

$$r = r(R, X) \tag{B.1}$$

$$\theta = \Theta \tag{B.2}$$

$$x = x(R, X). \tag{B.3}$$

We seek the transformations $r(R, X)$ and $x(R, X)$ that are solutions of the visco-plastic problem stated in Section 3.1, in the limit of slender bar, $\rho \ll L$. In a given cross-section, the variable X is fixed, and we assume the functions r and x can be both expanded with respect to R and ρ,

$$r(R, X) = \sum_{i,j \geq 0} r_{[i,j]}(X) \, \rho^i \, R^j$$
$$x(R, X) = \sum_{i,j \geq 0} x_{[i,j]}(X) \, \rho^i \, R^j$$

For the solution to be axisymmetric and smooth along the axis, $r(R, X)$ has to be an odd function of R and $x(R, X)$ an even function of R. As a result, $r_{[i,j]}(X) = 0$ if i is even, and $x_{[i,j]}(X) = 0$ whenever j is odd.

In the limit of a slender bar, $\rho \to 0$, and considering that R is of the same order as ρ, we can group terms in the expansions order by order in ρ,

$$r(R, X) = \qquad \rho r_{[0,1]}(X)\bar{R} \qquad + \qquad \rho^3\left(r_{[2,1]}(X)\bar{R} + r_{[0,3]}(X)\bar{R}^3\right) + \cdots$$
$$x(R, X) = x_{[0,0]}(X) \quad + \quad \rho^2(x_{[2,0]}(X) + x_{[0,2]}(X)\bar{R}^2) \qquad + \qquad \ldots$$

where the dots denote higher-order terms, and $\bar{R}$ denotes the dimensionless radial coordinate,

$$\bar{R} = \frac{R}{\rho}. \tag{B.4}$$

We define $\Lambda(X)$ as the x-coordinate of the average position of the material cross-section with initial coordinate X,

$$\Lambda(X) = \langle x \rangle(X), \tag{B.5}$$

where $\langle q \rangle(X) = \frac{1}{\pi \rho^2} \int_0^\rho q(X, R) \, 2\pi \, R \, dR$ denotes the cross-sectional average of a quantity $q(X, R)$.

The function $\Lambda(X)$ provides a one-dimensional version of the mapping from the reference to the current configuration. It will be the main kinematical quantity of the one-dimensional model.

Inserting the expansion of $x(R,X)$ into the right-hand side of (B.5), and identifying order by order with the left-hand side, we have

$$x_{[0,0]}(X) = \Lambda(X)$$

and $\langle x_{[2,0]}(X) + x_{[0,2]}(X)\,\bar{R}^2 \rangle = 0$. Using the geometric identity $\langle \bar{R}^2 \rangle = 1/2$ valid for circular cross-sections, this yields

$$x_{[2,0]}(X) = -\frac{x_{[0,2]}(X)}{2}. \tag{B.6}$$

In cylindrical coordinates, the expression of the transformation gradient $\underline{\underline{F}} = \underline{\nabla}\underline{x}$ is

$$\underline{\underline{F}} = \underline{e}_R \otimes \left(\frac{\partial r(X,R)}{\partial R} \underline{e}_R + \frac{\partial r(X,R)}{\partial X} \underline{e}_X \right) + \frac{r(X,R)}{R} \underline{e}_\Theta \otimes \underline{e}_\Theta$$
$$\ldots + \underline{e}_X \otimes \left(\frac{\partial x(X,R)}{\partial R} \underline{e}_R + \frac{\partial x(X,R)}{\partial X} \underline{e}_X \right). \tag{B.7}$$

At order $\rho^0 = 1$, $\underline{\underline{F}} = r_{[1,0]}(X) (\underline{e}_R \otimes \underline{e}_R + \underline{e}_\Theta \otimes \underline{e}_\Theta) + \frac{d\Lambda}{dX}(X) \underline{e}_X \otimes \underline{e}_X$ is diagonal. Therefore, the incompressibility condition $\det \underline{\underline{F}} = 1$ yields the transverse contraction (Poisson's effect) as

$$r_{[1,0]}(X) = \frac{1}{\sqrt{\lambda(X)}},$$

where $\lambda(X)$ is the macroscopic stretch, defined as

$$\lambda(X) = \frac{d\Lambda}{dX}(X). \tag{B.8}$$

Note that the macroscopic stretch $\lambda = d\langle x \rangle / dX = \langle dx/dX \rangle = \langle F_{xX} \rangle$ is also the cross-sectional average of the axial deformation gradient. It is *not* the average of the principal microscopic stretch, however, as we will show.

At this point, the transformation has been rewritten as

$$
\begin{array}{ccccccccc}
r(R,X) & = & 0 & + & \rho \frac{\bar{R}}{\sqrt{\lambda(X)}} & + & 0 & & + & \cdots \\
x(R,X) & = & \Lambda(X) & + & 0 & + & \rho^2 x_{[0,2]}(X) (\bar{R}^2 - \frac{1}{2}) & + & \cdots,
\end{array}
$$

The corresponding Green-St-Venant strain tensor $\underline{\underline{e}} = \frac{\underline{\underline{F}}^T \cdot \underline{\underline{F}} - 1}{2}$ can then be expanded in series as $\underline{\underline{e}}(R,X) = \underline{\underline{e}}_{[0]}(R,X) + \rho \, \underline{\underline{e}}_{[1]}(R,X) + \cdots$ where $\underline{\underline{e}}_{[0]}$ is diagonal and $\underline{\underline{e}}_{[1]}$ involves shear in the (x,r) plane,

$$\underline{\underline{e}}_{[0]}(R,X) = \frac{\lambda^2(X) - 1}{2} \underline{e}_X \otimes \underline{e}_X + \frac{\lambda^{-1}(X) - 1}{2} (\underline{e}_R \otimes \underline{e}_R + \underline{e}_\Theta \otimes \underline{e}_\Theta)$$

$$\underline{\underline{e}}_{[1]}(R,X) = \bar{R} \left[\lambda(X) x_{[0,2]}(X) - \frac{\lambda'(X)}{4\lambda^2(X)} \right] (\underline{e}_R \otimes \underline{e}_X + \underline{e}_X \otimes \underline{e}_R)$$

The first-order contribution $\underline{\underline{e}}_1$ is the dominant contribution to shear. Note that the square bracket in $\underline{\underline{e}}_{[1]}$ is a function of X only.

Both for a visco-plastic and an elastic material, the shear strain perpendicular to the lateral surface has to cancel by the traction-free boundary condition. This implies that $\underline{\underline{e}}_{[1]} = \underline{\underline{0}}$ whenever $\bar{R} = 1$. Since $\underline{\underline{e}}_{[1]}$ depend linearly on $\bar{R}$, this implies that the square bracket in the equation above vanishes: this yields $x_{[0,2]}(X)$ as

$$x_{[0,2]}(X) = \frac{\lambda'(X)}{4\lambda^3(X)} \tag{B.9}$$

As a result, the shear strain is zero in the entire bulk to first order in ρ, and not just at the lateral boundary,

$$\underline{\underline{e}}_{[1]}(R,X) = \underline{\underline{0}}. \tag{B.10}$$

The quantity $x_{[0,2]}(X) = \frac{\partial^2 x}{\partial R^2} + \mathcal{O}(\rho^2)$ measures the curvature of the deformed cross-sections. By Eq. (B.9), this curvature is adjusted so as to preserve orthogonality between the filaments that were initially radial and those that were parallel to the axis: when λ' is non-zero, there is a axial gradient in the transverse contraction of the cross-sections by Poisson's effect, and the material filaments initially perpendicular to the axis become convergent or divergent; as a result, the cross-sections bend out of their initial plane to preserve orthogonality with these material filaments. We have derived the same expression of the curvature of the cross-sections in the case of elastic necking (Audoly and Hutchinson, 2016).

At this point, we have completely determined the expansion of $r(R,X)$ and $x(R,X)$ in terms of the macroscopic stretch $\Lambda(X)$ up to order ρ^2 included. The third-order coefficients $r_{[2,1]}(X)$ and $r_{[0,3]}(X)$ can then be found from the incompressibility condition $\det \underline{\underline{F}} = 1$ at order ρ^2. This calculation is tedious but straightforward and the details are omitted. The final result is

$$r(R,X) = \frac{R}{\sqrt{\lambda(X)}} + \frac{(-3\rho^2 + 2R^2)R\lambda'^2(X) + (\rho^2 - R^2)R\lambda(X)\lambda''(X)}{16\lambda^{11/2}(X)} + \cdots$$

$$x(R,X) = \Lambda(X) + \frac{\lambda'(X)}{4\lambda^3(X)} \left(R^2 - \frac{\rho^2}{2} \right) + \cdots \tag{B.11}$$

This explicit 3D transformation depends only on the macroscopic stretch $\Lambda(X)$ and on its derivatives $\lambda(X) = \Lambda'(X)$ and $\lambda'(X) = \Lambda''(X)$. It is again straightforward but somewhat tedious to calculate the corresponding Green-St-Venant strain tensor to second order in ρ, which turns out to be diagonal at this order,

$$\underline{\underline{e}} = \frac{\lambda_R^2(R,X) - 1}{2} \underline{e}_R \otimes \underline{e}_R + \frac{\lambda_\Theta^2(R,X) - 1}{2} \underline{e}_\Theta \otimes \underline{e}_\Theta + \frac{\lambda_X^2(R,X) - 1}{2} \underline{e}_X \otimes \underline{e}_X + \mathcal{O}(\rho^3). \tag{B.12}$$

The vectors of the cylindrical basis $(\underline{e}_R, \underline{e}_\Theta, \underline{e}_X)$ are therefore the principal stretch directions (at least, at this order): this key remark will considerably simplify the dimensional reduction.

The corresponding principal stretches read

$$
\begin{aligned}
\lambda_R(R, X) &= \frac{1}{\sqrt{\lambda_e(X)}} + \rho^2 \lambda_\Delta(X) &&+ \left(R^2 - \frac{\rho^2}{2}\right)\delta_R(X) &&+ \mathcal{O}(\rho^3) \\
\lambda_\Theta(R, X) &= \frac{1}{\sqrt{\lambda_e(X)}} - \rho^2 \lambda_\Delta(X) &&+ \left(R^2 - \frac{\rho^2}{2}\right)\delta_\Theta(X) &&+ \mathcal{O}(\rho^3) \\
\lambda_X(R, X) &= \lambda_e(X) &&+ \left(R^2 - \frac{\rho^2}{2}\right)\delta_X(X) &&+ \mathcal{O}(\rho^3)
\end{aligned}
\tag{B.13}
$$

where we have introduced auxiliary functions, namely (*i*) the effective stretch

$$
\lambda_e(X) = \lambda(X) + \rho^2 \frac{\lambda'^2(X)}{16 \lambda^4(X)},
\tag{B.14}
$$

and (*ii*) the differential stretch $\lambda_\Delta(X)$, and (*iii*) the residual stretches $\delta_R(X)$, $\delta_\Theta(X)$ and $\delta_X(X)$,

$$
\begin{aligned}
\lambda_\Delta(X) &= \frac{3\,\lambda'^2(X) - \lambda(X)\,\lambda''(X)}{32\,\lambda^{11/2}(X)} \\
\delta_R(X) &= \frac{8\,\lambda'^2(X) - 3\,\lambda(X)\,\lambda''(X)}{16\,\lambda^{11/2}(X)} \\
\delta_\Theta(X) &= \frac{2\,\lambda'^2(X) - \lambda(X)\,\lambda''(X)}{16\,\lambda^{11/2}(X)} \\
\delta_X(X) &= \frac{-5\,\lambda'^2(X) + 2\,\lambda(X)\,\lambda''(X)}{8\,\lambda^4(X)}.
\end{aligned}
$$

These expressions of $\lambda_\Delta(X)$, $\delta_R(X)$, $\delta_\Theta(X)$ and $\delta_X(X)$ are given for the sake of completeness but do not enter into the 1D visco-plastic model at dominant order, as we will show.

Note that the terms $\left(R^2 - \frac{\rho^2}{2}\right)$ appearing in the principal stretches in (B.13) are all zero on average on any cross-section since $\langle R^2 \rangle = \rho^2/2$ in a disk of radius ρ. In particular, the last equation in (B.13) shows that the effective stretch λ_e is the cross-sectional average of the microscopic principal stretch λ_X measured along the material direction initially aligned with the axis. Eq. (B.14) however shows that this effective stretch λ_e is different from the quantity $\lambda(X)$, defined earlier as the derivative of the average cross-sectional axial coordinate $\Lambda(X)$: they differ by the gradient term $\rho^2 \lambda'^2/(16\,\lambda^2)$ accounting for the axial gradient of radial displacement.

The only assumption we have made so far is that the constitutive law and the equilibrium of the boundary force the shear-strain to cancel on the lateral boundary. In the following section, we focus to the case of a visco-plastic material.

B2. Application to the visco-plastic bar

For time-dependent problems, the kinematic analysis of the previous section is applicable at any time *t*. For the application to a visco-plastic bar, we need to restore the time parameter *t* in all previous expressions: the macroscopic variables $\Lambda(X, t)$, $\lambda(X, t)$ and $\lambda_e(X, t)$ are now functions of both the Lagrangian coordinate X and of t. We use primes for spatial derivatives (with respect to X) as earlier, and dots for time derivatives.

The visco-plastic model in Appendix A uses an Eulerian description of the motion, while the kinematic analysis of the cylinder in Section B.1 uses a Lagrangian description of motion. To connect them, we use the expression of the Eulerian strain rate $\underline{\dot{\varepsilon}}$ in terms of in terms of rate of change of the Lagrangian strain measure $\underline{\dot{e}}$ and of the deformation gradient $\underline{F}$ as $\underline{\dot{\varepsilon}} = \underline{F}^{-T} \cdot \underline{\dot{e}} \cdot \underline{F}^{-1}$. Based on this, the equivalent strain rate (3.1) reads

$$
\begin{aligned}
\dot{\varepsilon}_e(R, X, t) &= \left(\frac{2}{3}\,\operatorname{tr}(\underline{\underline{C}}^{-1} \cdot \underline{\underline{\dot{e}}} \cdot \underline{\underline{C}}^{-1} \cdot \underline{\underline{\dot{e}}})\right)^{1/2} \\
&= \left(\frac{2}{3}\left[\left(\frac{\dot{\lambda}_R}{\lambda_R}\right)^2 + \left(\frac{\dot{\lambda}_\Theta}{\lambda_\Theta}\right)^2 + \left(\frac{\dot{\lambda}_X}{\lambda_X}\right)^2\right]\right)^{1/2} + \mathcal{O}(\rho^3),
\end{aligned}
\tag{B.15}
$$

where $\underline{\underline{C}} = \underline{F}^T \cdot \underline{F}$ is the Green deformation tensor. To derive the second equality, we have used the important result that the matrices $\underline{\underline{C}} = 2\,\underline{\underline{e}} + \underline{\underline{I}}$ and $\underline{\underline{\dot{e}}}$ are both diagonal is the *same* frame ($\underline{e}_R$, $\underline{e}_\Theta$, $\underline{e}_X$), as the eigenvectors of $\underline{e}$ have a fixed direction relative to the cylindrical basis, see (B.12).

Inserting the expansion (B.13) of the principal stretches into this expression, expanding to second order in ρ, and averaging over the cross-section, we arrive at a very simple expression of the cross-sectional average of the effective strain rate:

$$
\langle \dot{\varepsilon}_e \rangle(X, t) = \frac{|\dot{\lambda}_e(X, t)|}{\lambda_e(X, t)} + \mathcal{O}(\rho^3) = \left|\frac{\partial \ln \lambda_e(X, t)}{\partial t}\right| + \mathcal{O}(\rho^3).
\tag{B.16}
$$

This formula plays a key role in the reduction to a one-dimensional model. It is remarkably simple thanks to the special form of the principal stretches in (B.13): all terms depending explicitly on R cancel out as they are proportional to $R^2 - \rho^2/2$,

the average of which is zero on a cross-section; the two terms depending on λ_Δ come with alternating signs and cancel each other as well.

By Eq. (3.2), the cross-sectional average of the cumulated elastic strain reads

$$\langle \varepsilon_e \rangle (X, t) = \int_0^t \left| \frac{\partial \ln \lambda_e(X, t')}{\partial t'} \right| \mathrm{d}t'. \tag{B.17}$$

If the effective stretch increases monotonously with time, *i.e.,* if $\dot\lambda_e(X, t)$ is always and everywhere positive, then the above relation can be integrated in time as

$$\langle \varepsilon_e \rangle (X, t) = \ln \lambda_e(X, t) \qquad \text{(monotonous stretching } \lambda_e). \tag{B.18}$$

This equation highlights the key role played by the effective strain in the visco-plastic bar model.

In addition, the previous analysis show that the difference between either $\dot\varepsilon_e$ or ε_e and their cross-sectional average can be written as

$$
\begin{aligned}
\dot\varepsilon_e(R, X, t) &= \langle \dot\varepsilon_e \rangle (X, t) + \left(R^2 - \frac{\rho^2}{2} \right) g(X, t) + \mathcal{O}(\rho^4) \\
\varepsilon_e(R, X, t) &= \langle \varepsilon_e \rangle (X, t) + \left(R^2 - \frac{\rho^2}{2} \right) h(X, t) + \mathcal{O}(\rho^4)
\end{aligned}
$$

for some residual functions g and h which we do not need to calculate. In view of this and of (3.4), the visco-plastic potential can be expressed in terms of the quantities of the one-dimensional model as

$$
\begin{aligned}
\Phi_{\varepsilon_e}(\dot\varepsilon_e) &= \iiint W_{\varepsilon_e}(\dot\varepsilon_e)\,\mathrm{d}x\mathrm{d}y\mathrm{d}z \\
&= \int \pi\,\rho^2 \langle W_{\varepsilon_e}(\dot\varepsilon_e) \rangle \mathrm{d}X \\
&= \int \pi\,\rho^2 \left(\left\langle W_{\langle \varepsilon_e \rangle}(\langle \dot\varepsilon_e \rangle) + \frac{\partial W_{\varepsilon_e}}{\partial \varepsilon_e}(\varepsilon_e - \langle \varepsilon_e \rangle) + \frac{\partial W_{\varepsilon_e}}{\partial \dot\varepsilon_e}(\dot\varepsilon_e - \langle \dot\varepsilon_e \rangle) \right\rangle \right) \mathrm{d}X + \mathcal{O}(\rho^4) \\
&= \int \pi\,\rho^2 \left(W_{\langle \varepsilon_e \rangle}(\langle \dot\varepsilon_e \rangle) + \frac{\partial W_{\varepsilon_e}}{\partial \varepsilon_e} \langle \varepsilon_e - \langle \varepsilon_e \rangle \rangle + \frac{\partial W_{\varepsilon_e}}{\partial \dot\varepsilon_e} \langle \dot\varepsilon_e - \langle \dot\varepsilon_e \rangle \rangle \right) \mathrm{d}X + \mathcal{O}(\rho^4) \\
&= \int \pi\,\rho^2 \left(W_{\langle \varepsilon_e \rangle}(\langle \dot\varepsilon_e \rangle) + \frac{\partial W_{\varepsilon_e}}{\partial \varepsilon_e} \underbrace{\left\langle R - \frac{\rho^2}{2} \right\rangle}_{0} h(X, t) + \frac{\partial W_{\varepsilon_e}}{\partial \dot\varepsilon_e} \underbrace{\left\langle R - \frac{\rho^2}{2} \right\rangle}_{0} g(X, t) \right) \mathrm{d}X + \mathcal{O}(\rho^4) \\
&= \int \pi\,\rho^2 W_{\langle \varepsilon_e \rangle}(\langle \dot\varepsilon_e \rangle)\,\mathrm{d}X + \mathcal{O}(\rho^4)
\end{aligned} \tag{B.19}
$$

To derive the second equality above, we have used the incompressibility $\mathrm{d}x\mathrm{d}y\mathrm{d}z = \pi\,\rho^2\mathrm{d}X$.

In view of the equation above, we can simply substitute the *cross-sectional averages* of the cumulated elastic strain and of the equivalent strain rate into the 3-d visco-plastic potential, to obtain an effective visco-plastic potential $\Phi_\lambda(\dot\lambda)$ governing the one-dimensional problem,

$$\Phi_\lambda(\dot\lambda) = \int \pi\,\rho^2 W_{\langle \varepsilon_e \rangle}(\langle \dot\varepsilon_e \rangle)\,\mathrm{d}X.$$

For the 3-d visco-plastic model defined in (3.5) for instance, the one-dimensional potential takes the form

$$\Phi_\lambda(\dot\lambda) = \int_0^L \pi\,\rho^2 \frac{K \langle \varepsilon_e \rangle^N \langle \dot\varepsilon_e \rangle^{m+1}}{m+1}\,\mathrm{d}X.$$

All the results of this section are summarized in Section 3.2, with two small changes: the square brackets for the cross-sectional averages $\langle \ldots \rangle$ are dropped out for the sake of readability, and an imperfection factor $f(X)$ is introduced, *i.e.,* the undeformed cross-sectional area $\pi\rho^2$ is replaced with $\pi\rho^2 f$.

Appendix C. Recovering the 1D rate-independent model from previous work

In our previous work, we have used an asymptotic method to derive a one-dimensional model for the analysis of necking in a rate-independent cylinder (Audoly and Hutchinson, 2016). This one-dimensional model retains both the dominant contribution to the strain energy arising from the stretch $\lambda(X)$, and the sub-dominant contribution arising from the stretch *gradient* λ'. The latter is important for the analysis of localization.

Here, we show that this one-dimensional model for a non-linear elastic bar can be derived easily from the expression of the effective stretch λ_e which we have established in (B.14).

For the sake of simplicity, we limit attention to a prismatic bar having a circular cross-section with radius ρ, made of a homogeneous and isotropic material. Consider the solution for simple traction (uniaxial stress parallel to the axis) with an axial stretch λ. Let $W_h(\lambda)$ denote the strain energy of this homogeneous solution per unit volume of the bar.

In the presence of stretch gradients, a calculation similar to that presented in (B.19) shows that the strain energy in the bar can be approximated by the integral of the homogeneous strain energy W_h, in which the homogeneous stretch λ has been substituted with the *effective* stretch λ_e,

$$\Phi(\lambda) = \int_0^L W_h(\lambda_e)\mathrm{d}X. \tag{C.1}$$

The effective stretch λ_e is given by (B.14) as $\lambda_e(X) = \lambda(X) + \rho^2 \frac{\lambda'^2(X)}{16\,\lambda^4(X)}$. In the equation above, the expression of the integrand $W_h(\lambda_e)$ can be justified using the two following arguments. The microscopic strain remains uniaxial and aligned with the axial material up to order $(\rho/R)^2$ included, which explains why the strain energy can be expressed in terms of the energy of homogeneous solutions W_h. In addition, λ_e is the cross-sectional average of the stretch along the filaments that were initially parallel to the axis of the bar, as noted earlier, which is why the argument of W_h is λ_e.

To show the equivalence of the strain energy (C.1) with that derived in our earlier work, we simply expand the former with respect to the small parameter ρ^2,

$$\Phi(\lambda) = \int_0^L \left[W_h(\lambda) + \frac{(2\rho)^2}{2} W_h'(\lambda) \frac{\lambda'^2(X)}{32\,\lambda^4(X)} \right] dX$$

up to terms of order ρ^4 or higher. When $W_h'(\lambda)$ is identified with the axial force needed to achieve a homogeneous, axial stretch λ, the strain energy Φ above is seen to be equivalent to equation [1.4] of our previous paper (Audoly and Hutchinson, 2016).

Appendix D. Dimension reduction for a sheet in generalized plane-strain

D1. Kinematic analysis for a sheet

The dimension reduction done in Appendix B for a cylinder can be adapted to the case of a sheet undergoing generalized plane strain as follows.

Let (X, Y, Z) denote the Cartesian coordinates in undeformed configuration, with 2ρ denoting the initial thickness of the sheet. Let $\underline{x} = (x(X,Y), y(X,Y), z(Z))$ denote a point in deformed configuration. According to the generalized plane strain assumption, a uniform stretch is imposed in the transverse direction,

$$z(Z) = aZ$$

where a is the stretch along the neck. While the stretch will ultimately be a function of time $a(t)$, we start by a kinematic analysis of the sheet at fixed time t and ignore any dependence on t for the moment (Fig. D.15).

The solution of the 3D visco-plastic flow is sought as an expansion in terms of the small thickness ρ as earlier, taking the top-down symmetry into consideration,

$$x(X,Y) = x_{[0,0]}(X) \quad + \quad \rho^2(x_{[2,0]}(X) + x_{[0,2]}(X)\bar{Y}^2) \qquad + \qquad \cdots$$
$$y(X,Y) = \quad \rho y_{[0,1]}(X)\bar{Y} \qquad + \qquad \rho^3\left(\ y_{[2,1]}(X)\bar{Y} \ + r_{[0,3]}(X)\bar{Y}^3 \right) + \cdots$$

where $\bar{Y}$ denotes the scaled transverse coordinate,

$$\bar{Y} = \frac{Y}{\rho}.$$

As earlier, we denote by $\Lambda(X)$ the average x-coordinate of the cross-section labelled by X, and by $\lambda(X) = \frac{d\Lambda}{dX}(X)$ the stretch. Denoting by $\langle \cdot \rangle$ the cross-sectional average, the identity $\Lambda(X) = \langle x(X,Y) \rangle$ yields, at orders ρ^0 and ρ^2 respectively,

$$x_{[0,0]}(X) = \Lambda(X)$$
$$x_{[0,2]}(X) = -\frac{x_{[0,2]}(X)}{3}$$

The incompressibility condition at order ρ^0 yields
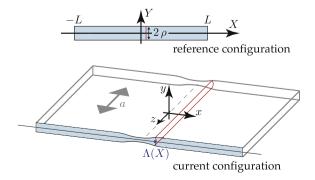
$$y_{[0,1]}(X) = \frac{1}{a\lambda(X)},$$

Fig. D.15. Necking of a sheet in generalized plain strain: notation used in the Appendix.

where $\lambda(X)$ is the apparent macroscopic stretch defined earlier in (B.8).

The Green-St-Venant strain tensor $\underline{\underline{e}} = \frac{\underline{\underline{F}}^T \cdot \underline{\underline{F}} - \underline{\underline{1}}}{2}$ has to cancel at order ρ^1 by the same argument as earlier. This yields

$$x_{[0,2]}(X) = \frac{\lambda'(X)}{2a^2\lambda^4(X)},$$

which sets the curvature of the cross-sections in deformed configuration.

Finally, the incompressibility condition at order ρ^2 set the coefficients $x_{[2,1]}(X)$ and $x_{[0,3]}(X)$ and we find the deformed configuration as

$$x(R,X) = \Lambda(X) \quad - \quad \frac{\lambda'(X)}{6a^2\,\lambda^4(X)}\,(\rho^2 - 3Y^2) \quad + \quad \cdots$$

$$r(R,X) = \quad \frac{Y}{a\lambda(X)} \quad + \quad \frac{(-4\rho^2 + 2Y^2)Y\lambda'^2(X) + (\rho^2 - Y^2)Y\lambda(X)\lambda''(X)}{6a^3\lambda^7(X)} + \cdots$$

We find again that the Green-St-Venant strain tensor is diagonal in the Cartesian coordinate basis up to order ρ^2 included, and we calculate the corresponding principal stretches as

$$
\begin{array}{rcccccl}
\lambda_X(X,Y) & = & \lambda_e(X) & + & (\rho^2 - 3Y^2)\,\delta_X(X) & + & \mathcal{O}(\rho^3) \\
\lambda_Y(X,Y) & = & \frac{1}{a\lambda_e(X)} & + & (\rho^2 - 3Y^2)\,\delta_Y(X) & + & \mathcal{O}(\rho^3) \\
\lambda_Z(X,Y) & = & a & + & 0 & + & \mathcal{O}(\rho^3)
\end{array}
\tag{D.1}
$$

where we have introduced auxiliary functions, namely (*i*) the effective stretch

$$\lambda_e(X) = \lambda(X) + \rho^2\,\frac{\lambda'^2(X)}{6a^2\,\lambda^5(X)},\tag{D.2}$$

and (*ii*) the residual stretches $\delta_X(X)$, $\delta_Y(X)$,

$$\delta_X(X) = \frac{3\,\lambda'^2(X) - \lambda(X)\,\lambda''(X)}{6a^2\,\lambda^5(X)}$$

$$\delta_Y(X) = \frac{-3\,\lambda'^2(X) + \lambda(X)\,\lambda''(X)}{6a^3\,\lambda^7(X)}.$$

In Eq. (D.1), the dependence on the transverse coordinate Y takes place through the factors $(\rho^2 - 3Y^2)$ which cancel when averaged over the sheet thickness. This warrants that the residual stretches $\delta_X(X)$, $\delta_Y(X)$ disappear from the macroscopic quantities that we calculate next, as with the axisymmetric bar.

Restoring the dependence on time t which has been omitted so far, we can calculate the cross-section average of the equivalent strain rate $\dot{\varepsilon}_e$ using (B.15) as

$$
\begin{array}{rcl}
\langle\dot{\varepsilon}_e\rangle(X,t) & = & \left(\frac{2}{3}\left[\left(\frac{\dot\lambda_X}{\lambda_X}\right)^2 + \left(\frac{\dot\lambda_Y}{\lambda_Y}\right)^2 + \left(\frac{\dot\lambda_Z}{\lambda_Z}\right)^2\right]\right)^{1/2} \\[3mm]
& = & \left(\frac{2}{3}\left[\left(\frac{\dot\lambda_e}{\lambda_e}\right)^2 + \left(\frac{\dot\lambda_e}{\lambda_e} + \frac{\dot a}{a}\right)^2 + \left(\frac{\dot a}{a}\right)^2\right]\right)^{1/2} \\[3mm]
& = & \left(\frac{4}{3}\left[\left(\frac{\dot\lambda_e}{\lambda_e}\right)^2 + \frac{\dot\lambda_e}{\lambda_e}\frac{\dot a}{a} + \left(\frac{\dot a}{a}\right)^2\right]\right)^{1/2}
\end{array}
\tag{D.3}
$$

Note that the equivalent elastic strain is now history-dependent, and must be calculated by integrating over time,

$$\langle\varepsilon_e\rangle(X,t) = \int_0^t \langle\dot{\varepsilon}_e\rangle(X,t')\,\mathrm{d}t'.\tag{D.4}$$

D2. Application to the visco-plastic sheet

By the same argument as earlier in Appendix B.2, the visco-plastic sheet is governed by a one-dimensional potential

$$\Phi_\lambda(\dot\lambda) = \int_0^L (2\,\rho)D\frac{K\,\langle\varepsilon_e\rangle^N\,\langle\dot{\varepsilon}_e\rangle^{m+1}}{m+1}\,\mathrm{d}X.\tag{D.5}$$

In this expression, one should insert the expressions of $\langle\dot{\varepsilon}_e\rangle$, $\langle\varepsilon_e\rangle$ and λ_e derived in the previous section, as summarized in Section 3.3. In the main text, we use these expressions in the particular case of a plane-strain sheet, $a = 1$ and $\dot a = 0$.

Appendix E. Numerical method for solving the rate problem using splines

The non-dimensional quantities introduced in Sections 4 and 5 are used here. Divide the interval $(0, L)$ into $n_s - 1$ equally spaced intervals with nodes X_i ($i = 1, \ldots, n_s$) and employ n_s splines $S_i(X)$ each defined on $(0,L)$ to represent the stretch distribution as

$$\lambda(X) = \sum_{i=1}^{n_s} a_i S_i(X) \tag{E.1}$$

where $a_i = \lambda(X_i)$. Conditions at the bar ends require $S_i'(0) = 0$ for $i = 1, \ldots, n_s$. The amplitudes a_i are regarded as functions of time such that the stretch-rate is $\dot{\lambda}(X) = \sum_{i=1}^{n_s} \dot{a}_i S_i(X)$. The prescribed average stretch-rate, $\dot{\lambda}_{ave}$, requires

$$\sum_{i=1}^{n_s} \dot{a}_i (S_i)_{ave} = \dot{\lambda}_{ave} \quad \text{with } (S_i)_{ave} = \frac{1}{L} \int_0^L S_i(X) dX \tag{E.2}$$

Denote the value of the first term of stretch-rate functional Φ in (4.5) by $F(\dot{a})$ when evaluated using the spline representation, with the dependence on the current stretch amplitudes, a, and the other parameters left implicit. Thus, (4.5) becomes

$$\Phi(\dot{a}) = F(\dot{a}) - \zeta \left(\sum_{i=1}^{n_s} \dot{a}_i (S_i)_{ave} - \dot{\lambda}_{ave} \right) \tag{E.3}$$

Stationarity of Φ with respect to the $\dot{a}_i$ requires

$$\frac{\partial F}{\partial \dot{a}_i} = -\zeta (S_i)_{ave} \quad \text{for } i = 1, \ldots, n_s \tag{E.4}$$

Enforcing (E.2) gives

$$\frac{\partial F}{\partial \dot{a}_i} - \frac{(S_i)_{ave}}{\dot{\lambda}_{ave}} \sum_{j=1}^{n_s} \dot{a}_j \frac{\partial F}{\partial \dot{a}_j} = 0 \quad \text{for } i = 1, \ldots, n_s \tag{E.5}$$

Newton's iterative method is used to solve (E.5) for $\dot{a}$ at each step of the overall loading. With $\dot{a}$ denoting an estimate of the solution in the current iteration and $\dot{a} + \delta \dot{a}$ denoting the estimate in the next iteration, $\delta \dot{a}$ is given by

$$\sum_{j=1}^{n_s} M_{ij} \delta \dot{a}_j = -\frac{\partial F}{\partial \dot{a}_i} + \frac{(S_i)_{ave}}{\dot{\lambda}_{ave}} \sum_{j=1}^{n_s} \dot{a}_j \frac{\partial F}{\partial \dot{a}_j} = 0 \quad \text{for } i = 1, \ldots, n_s \tag{E.6}$$

with

$$M_{ij} = \frac{\partial^2 F}{\partial \dot{a}_i \partial \dot{a}_j} - \frac{(S_i)_{ave}}{\dot{\lambda}_{ave}} \left(\frac{\partial F}{\partial \dot{a}_j} + \sum_{k=1}^{n_s} \dot{a}_k \frac{\partial^2 F}{\partial \dot{a}_j \partial \dot{a}_k} \right) \tag{E.7}$$

The converged solution $\dot{a}$ is used to increment the stretch for the next step according to $a + \dot{a} \to a$.

In each iteration, F and its partial derivatives are evaluated numerically in a straightforward manner exploiting the spline representation. The estimate of $\dot{a}$ in the first iteration of any step of loading is taken to be the converged solution in the prior step, scaled accordingly if the prescribed overall stretch increment changes. The only exception in this incremental procedure is for the first step starting from the unstressed bar. For this starting step, the long-wavelength solution is used to generate the solution at $\lambda_{ave} = 1 + \Delta \lambda_{ave}$ where $\Delta \lambda_{ave}$ is small compared to the stretch at necking. We have established the accuracy of this starting step by repeating the necking calculations with various choices of $\Delta \lambda_{ave}$ and showing that the necking prediction is insensitive to the choice.

Appendix F. Simplified analysis of the gradient effect

In this Appendix, we propose a simplified analysis of neck growth for sheets necking in-plane strain (or in a long round bar with a 'local' imperfection) that brings in the lower order effects of the gradients.

We will consider a sheet (or round bar) with imperfection wavelength sufficiently small, i.e., $\ell/L \ll 1$, such that well outside the necking region the straining is uniform. In the notation used in the body of the paper, the dimensionless thickness imperfection (or dimensionless area imperfection for the bar) is taken to be $f(X) = 1 - \eta e^{-\left(\frac{X}{\ell}\right)^2}$. The sheet or bar is again symmetric with respect to $X = 0$ and we denote quantities evaluated at $X = L$ by a subscript or superscript 'B'. The strain-rate potential is $W = \varepsilon_e^N \dot{\varepsilon}_e^{m+1}/(m+1)$. Taking $f^2 = 1$ in the gradient stretch contribution ($f = 1$ for the bar), one has

$$\varepsilon_e = c_1 \ln \lambda_e \quad \lambda_e = \lambda + c_2 \lambda'^2 / \lambda^s \quad \dot{\varepsilon}_e = c_1 \dot{\lambda}_e / \lambda_e \quad \dot{\lambda}_e = (s c_2 \lambda'^2 + \lambda^{s+1}) \dot{\lambda} + 2 c_2 \lambda' \dot{\lambda}' / \lambda^s.$$

where $\left(c_1 = 2/\sqrt{3}, c_2 = 1/24, s = 5\right)$ for the sheet and $(c_1 = 1, c_2 = 1/16, s = 4)$ for the round bar. The nonlinear o.d.e. associated with $\delta\Phi = 0$, assuming L is sufficiently large such that the solution has attained uniform straining at $X = L$,

$$-\left(\frac{2c_2 f \tau \lambda'}{\lambda^s}\right)' + f\tau\left(1 - \frac{sc_2 + \lambda'^2}{\lambda^{s+1}}\right) = \tau_B \quad \text{with } \lambda' = 0 \text{ at } X = 0, L \tag{F.1}$$

and where $\tau = \partial W / \partial \dot{\lambda}_e = c_1 \varepsilon_e{}^N \dot{\varepsilon}_e{}^{m+1} / \lambda_e$.

We will regard the loading parameter to be the uniform stretch-rate at $X = L$, $\dot{\lambda}_B$, with the notation: $\varepsilon_e^B = c_1 \ln \lambda_B$, $\dot{\varepsilon}_e^B = c_1 \dot{\lambda}_B / \lambda_B$, $f_B = 1$, $\tau_B = c_1 \left(\varepsilon_e^B\right)^N \left(\dot{\varepsilon}_e^B\right)^m / \lambda_B$, etc. In what follows, we take

$$f = 1 - \eta \Delta f(X) \quad \lambda = \lambda_B + \eta \Delta\lambda(X) \quad \text{and} \quad \dot{\lambda} = \dot{\lambda}_B + \eta \Delta\dot{\lambda}(X). \tag{F.2}$$

Neglecting terms of order η^2, the first term in (F.1) can be replaced by $-2\eta c_2 \tau_B \Delta\lambda'' / \lambda_B{}^s$ and the second term becomes $f\tau$, such that the approximation to (F.1) is

$$f\tau = \tau_B + \eta \tau_B \frac{2c_2 \Delta\lambda''}{\lambda_B{}^s}. \tag{F.3}$$

As it stands, (F.3) is the un-approximated long-wavelength equation with the stretch given by $\lambda = \lambda_B + \eta\Delta\lambda(X)$ if the term involving $\Delta\lambda''$ is omitted. This equation can be solved for the strain-rate distribution giving

$$\dot{\varepsilon}_e = \left[\frac{1}{f}\frac{\lambda_e}{\lambda_B}\left(\frac{\varepsilon_e^B}{\varepsilon_e}\right)^N \left(1 + \eta \frac{2c_2 \Delta\lambda''}{\lambda_B{}^s}\right)\right]^{1/m} \dot{\varepsilon}_e^B.$$

The final step is to use $\dot{\varepsilon}_e = c_1\left(\dot{\lambda}_B + \eta\Delta\dot{\lambda}\right)/(\lambda_B + \eta\Delta\lambda)$ to solve for the equation governing $\Delta\dot{\lambda}$

$$\Delta\dot{\lambda} = \frac{1}{\eta}\left\{\left(1 + \frac{\eta\Delta\lambda}{\lambda_B}\right)\left[\frac{1}{f}\left(1 + \eta\frac{\Delta\lambda}{\lambda_B}\right)\left(\frac{\varepsilon_e^B}{\varepsilon_e}\right)^N \left(1 + \frac{2\eta c_2 \Delta\lambda''}{\lambda_B{}^s}\right)\right]^{1/m} - 1\right\}\dot{\lambda}_B \tag{F.4}$$

where λ_e has been replaced by $\lambda_B + \eta\Delta\lambda$ neglecting terms of order $\eta^2 \Delta\lambda'^2$ and smaller.

With $\Delta\lambda''$ set to zero, (F.4) is precisely the long-wavelength approximation with $\lambda = \lambda_B + \eta\Delta\lambda$ as the stretch. In other words, (F.4) brings in the lowest order correction of the long-wavelength approximation due to stretch gradients. This recipe is an explicit formula for expressing the increments of stretch distribution in terms of $\dot{\lambda}_B$ and the current distributions of $\Delta\lambda$ and $\Delta\lambda''$, which are both zero when $\lambda_B = 1$. It can be implemented in a straightforward manner incrementally step by step for increasing λ_B. Some care must be exercised to ensure that the calculation of $\Delta\lambda''$ does not destabilize the numerical solution. At each step, we have used a cubic spline representation of $\Delta\lambda$ at equally spaced points on the interval $0 \le X \le L$ and computed $\Delta\lambda''$ from that representation. Predictions using this simple approximation are included in Fig. 12 for plane strain sheet necking where it is seen that it retains good accuracy for growth of the neck to more than thirty times the initial deficit. It is equally effective for the round bar when the width of the initial imperfection is on the order of the diameter of the bar, as seen in Fig. 8.

References

Audoly, B., Hutchinson, J.W., 2016. Analysis of necking based on a one-dimensional model. J. Mech. Phys. Solids 97, 68–91.

Bridgman, P.W., 1952. Studies in large plastic flow and fracture. In: Metallurgy and Metallurgical Engineering Series. McGraw-Hill, New York.

Christoffersen, J., Hutchinson, J.W., 1979. A class of phenomenological corner theories of plasticity. J. Mech. Phys. Solids 27 (5), 465–487.

Ghosh, A.K., 1977. Tensile instability and necking in materials with strain hardening and strain-rate hardening. Acta Metall. 12 (25), 1413–1424.

Hutchinson, J.W., Neale, K.W., 1977. Influence of strain-rate sensitivity on necking under uniaxial tension. Acta Metall. 25, 839–846.

Hutchinson, J.W., Neale, K.W., Koistinen, D.P., Wang, N.M., 1978a. Sheet necking—III. Strain-rate effects. In: Mechanics of Sheet Metal Forming: Material Behavior and Deformation Analysis. Springer US, Boston, MA, pp. 269–285.

Hutchinson, J.W., Neale, K.W., Koistinen, D.P., Wang, N.M., 1978b. Sheet necking—II. Time-independent behavior. In: Mechanics of Sheet Metal Forming: Material Behavior and Deformation Analysis. Springer US, Boston, MA, pp. 127–153.

Johnson, G.R., Cook, W.H., 1985. Fracture characteristics of three metals subjected to various strains, strain rates, temperatures and pressures. Eng. Fract. Mech. 21, 31–48.

Marciniak, Z., Kuczyński, K., Pokora, T., 1973. Influence of the plastic properties of a material on the forming limit diagram for sheet metal in tension. Int. J. Mech. Sci. 15 (10), 789–800.

Stören, S., Rice, J.R., 1975. Localized necking in thin sheets. J. Mech. Phys.Solids 23, 421–441.

Woodford, D.A., 1969. Strain-rate sensitivity as a measure of ductility. Am. Soc. Metals Trans. Q. 62, 291–293.